

ARTICLE INFO

Article ID: 04-16-02-0009 © 2023 SAE International doi:10.4271/04-16-02-0009

Partially Premixed Combustion Study between n-Butanol and Ethanol for the Reduction of NOx and Nonrenewable Carbon Emissions

Valentin Soloiu,1 Cesar Carapia,2 Richard Smith,2 Amanda Weaver,2 Lily Parker,2 Dillan Brock,2 Levi Mckinney,2 Gustavo Molina,² and Marcel Ilie²

¹Georgia Southern University, Mechanical Engineering, USA

Abstract

A comprehensive study was conducted in an experimental engine, on the combustion/emissions characteristics of Partially Premixed Combustion (PPC) with either n-butanol or ethanol at either 30% or 40% Port Fuel Injection (PFI) by mass, and Conventional Diesel Combustion (CDC) was used to compare the performance of each PPC test conducted.

It was found in the combustion analysis that PPC with either n-butanol or ethanol had several advantageous combustion characteristics compared to CDC, such as Peak Pressure Rise Rate (PPRR, bar/CAD), Ringing Intensity (RI, MW/m²), and Apparent Heat Release Rate (AHRR). As the load was increased, Low Temperature Heat Release (LTHR) and Negative Temperature Coefficient (NTC) regions were extended for PPC with n-butanol when comparing PPC with ethanol. Although PPC consisted of 30% and 40% low-reactivity PFI fuel by mass, combustion pressure was observed to have similar peak values with CDC experiments. It was found that as the PFI percentage (%) increased, peak pressure increased for PPC with either n-butanol or ethanol and only PPC 40BU reached a peak pressure greater than CDC at 67.8 bar.

It was found that the PPRR and RI for PPC with ethanol were higher than PPC with n-butanol at both 30% and 40% PFI by mass. The PPRR values at a load of 4 bar and 5 bar Indicated Mean Effective Pressure (IMEP) for n-butanol at a 30% PFI are 2.3 bar/CAD and 3.4 bar/CAD, respectively, and the values with 40% PFI are 2.9 bar/CAD and 2.8 bar/CAD, respectively. The PPRR values at a load of 4 bar and 5 bar IMEP for ethanol at a 30% PFI are 2.6 bar/CAD and 5.0 bar/CAD, respectively, and the values with 40% PFI are 4.7 bar/CAD and 5.5 bar/ CAD, respectively.

The RI values at a load of 4 bar and 5 bar IMEP for n-butanol at a 30% PFI are 0.15 MW/m² and 0.39 MW/ m², respectively, where the RI values at 40% PFI of n-butanol are 0.39 MW/m² and 0.15 MW/m², respectively. The RI values at a load of 4 bar and 5 bar IMEP for ethanol at a 30% PFI are 0.35 MW/m² and 0.69 MW/m², respectively, whereas the RI values at 40% PFI of n-butanol are 0.75 MW/m² and 0.64 MW/m², respectively.

In PPC mode, PPRR and RI remained lower than in CDC mode. At 4 bar and 5 bar IMEP, CDC has values of 1.48 MW/m^2 and 1.32 MW/m^2 for RI, respectively. The CDC values for PPRR for CDC in 4 bar and 5 bar are 5.79 bar/CAD and 6.76 bar/CAD, respectively. PPC reduced Nitrogen Oxides (NOx) and soot emissions significantly compared to CDC. The 40BU resulted in the greatest NOx emissions reduction of 62.06% (-9.31 g/kWh) at 5 bar IMEP compared to CDC, respectively. The 40ET achieved the lowest soot emissions with reductions of 84.71% (-1.48 g/kWh) at 5 bar IMEP compared to CDC. Additionally, the nonrenewable carbon was reduced at a load of 5 bar IMEP by 15.3% for PPC 30ET and 38.8% for PPC 40BU. As is typical with Low Temperature Combustion (LTC) methods such as PPC, the reduction of NOx and soot emissions come at the cost of Unburnt Hydrocarbon (UHC) emissions and Carbon Monoxide (CO) emissions. In this study, it was observed that PPC had higher emission outputs of UHC and CO than CDC.

History

Received: 31 Mar 2022 12 Jul 2022 Revised: Accepted: 25 Oct 2022 e-Available: 19 Dec 2022

Keywords

PPC, GHG, Bio-alcohols, n-Butanol, PPRR

Citation

Soloiu, V., Carapia, C., Smith, R., Weaver, A. et al., "Partially Premixed Combustion Study between n-Butanol and Ethanol for the Reduction of NOx and Nonrenewable Carbon Emissions," SAE Int. J. Fuels Lubr. 16(2):2023, doi:10.4271/04-16-02-0009.

ISSN: 1946-3952 e-ISSN: 1946-3960

This article is part of a Special Issue on Fuels and Combustion Control Strategies for Low Temperature Combustion Engines.









²Georgia Southern University, USA

Novel Combustion Methods for Climate Change Mitigation

n recent times, more attention have been drawn to mitigating the impact various power/transportation platforms have on climate change when using alternative fuels. As a result, emissions regulations have become more stringent, with some markets proposing the banning of Internal Combustion Engine (ICE)-powered passenger vehicles [1]. However, ICEs will remain an integral part of society's power/transportation needs in the foreseeable future for heavy-duty propulsion and power generation applications; thus, research is needed to further mitigate the impact on climate change.

To reduce humanity's impact on the climate, research is underway for the use of Advanced Combustion Techniques (ACTs) in conjunction with various biofuels for the reduction of emissions produced by ICEs. Various Low Temperature Combustion (LTC) methods have been utilized in previous investigations to simultaneously reduce Nitrogen Oxides (NOx) and soot/Particulate Matter (PM) emissions. Dahodwala et al. used Reactivity Controlled Compression Ignition (RCCI) with Compressed Natural Gas (CNG), D'Ambrosio et al. and Sun et al. investigated Premixed Charge Compression Ignition (PCCI) using high quantities of Exhaust Gas Recirculation (EGR), D'Ambrosio et al. optimized PCCI utilizing regression models, Rohani et al. investigated injection strategies to optimize PCCI, Musculus et al. modeled Partially Premixed Combustion (PPC) with 10-15% oxygen air content, and Cui et al. investigated Homogeneous Charge Compression Ignition (HCCI) and PPC under transitory conditions [2, 3, 4, 5, 6, 7, 8]. Although LTC methods have been shown to reduce emissions, each method operates at ideal ranges in order to maintain combustion stability. HCCI, PCCI, and PPC are optimal at low to medium loads (dependent on fuel used) as seen in investigations by Cui et al. with HCCI, Singh et al. with PCCI, Pandey et al. with PCCI, Soloiu et al. with PCCI, and Chu et al. with Dual-Fuel Premixed Charge Compression Ignition (DF-PCCI) [8, 9, 10, 11, 12, 13]. RCCI, however, has an optimal load range from mid to high engine loads as seen by Singh et al. and Dahodwala et al., with stable ranges differing based on the utilized fuels [2, 9].

However, greater emissions reductions and combustion stability can be achieved with the use of two fuels rather than one in LTC methods such as DF-PCCI, PPC, and RCCI. The use of oxygenated biofuels provides the greatest benefit for reducing soot emissions. This reduction comes from the additional molecular oxygen available in the fuel requiring the engine to be less dependent on ambient air for oxygen. As ambient air contains nitrogen, the use of oxygenated biofuels reduces NOx emissions. In addition to the reduction of emissions produced from combustion, biofuels have greater potential in mitigating climate change through their participation in the carbon cycle, thus reducing the quantity of previously locked-away carbon from getting into the atmosphere. Martin

et al. investigated the environmental impact and optimal configuration of biofuels for a case study in Spain whereas Morales et al. investigated the life cycle of lignocellulosic bioethanol impact on the environment [14, 15]. In addition, advancements have been made in the production of drop-in biofuels for both consumer and commercial markets as seen by Kargbo et al. and Braz et al. [16, 17].

LTC Methods (PCCI, RCCI, HCCI)

ACTs have great potential for NOx and PM reduction simultaneously. Single-fueled and dual-fueled ACTs such as HCCI, PCCI, and DF-PCCI. Results show that these three ACTs could reduce the NOx and PM emissions generated by a heavyduty diesel engine simultaneously without aftertreatment systems. HCCI and PCCI single-fueled combustion required EGR above 40% and a multiple-injection strategy to match the optimum combustion phase for the best thermal efficiency. DF-PCCI generated 45.3% indicated thermal efficiency and reduced Carbon Dioxide (CO₂) emissions by 14.3% under low load with a 40% substitution ratio of natural gas. DF-PCCI combustion produced nearly 7.8 times the amount of Total Hydrocarbon (THC) emissions than CDC but was lower still than single-fueled ACTs [18].

Analysis was conducted on a Liquefied Petroleum Gas (LPG)-fueled HCCI engine with manifold LPG injection and pilot Direct Injection (DI) diesel injection. Hydrocarbon (HC) emissions in LPG mode were found to be higher at 125.5g/kWh when compared with diesel at just 5.37 g/kWh. This is due to the poor combustion of the gaseous fuel at low loads. NOx emissions were determined to be 60% less for HCCI with LPG in comparison to diesel at full load. Brake Specific Fuel Consumption (BSFC) was found to be less with LPG than with neat diesel operation under all load conditions [19].

A numerical study was conducted to compare the PCCI combustion performance and emissions characteristics of neat biodiesel (B100) to a blend of 20% biodiesel and 80% diesel (B20). Simulated engine conditions were set to 2000 rpm and 5.5 bar Indicated Mean Effective Pressure (IMEP). It was found that the NOx concentrations for B20 and B100 were significantly lower for both fuels. The Indicated Specific Fuel Consumption (ISFC) of B100 was consistently higher than that of B20, up to 8% higher [20].

When a modified Common Rail Direct Injection (CRDI) research engine utilized RCCI combustion running on biodiesel with isopropanol-butanol-ethanol, it was found that in-cylinder peak pressure decreased by 4.8% compared to petroleum diesel [1]. The use of low-reactivity fuel successfully reduced NOx emissions by 40% at 20% load. At higher premixed ratios, NOx emissions were observed to increase [21].

A turbocharged RCCI engine is analyzed at different operating conditions with diesel and hydrogen as fuels. Due to increased Combustion Duration (CD), pressure is reduced in the combustion chamber and ISFC is decreased by 2.9% compared to CDC [22].

The comparison of diesel-gasoline RCCI versus CDC demonstrated the superior capacity of RCCI in exploiting the energy released from fuel combustion. The short CD compared to CDC resulted in a reduction of 13% in the heat transfer values. Moreover, the low enthalpy of the exhaust gas with RCCI leads to lower exhaust losses than CDC. Nonetheless, the combustion efficiency values are still low compared to the CDC and the improvement of this parameter is still a challenge in RCCI combustion [23].

Nishida et al. [24] studied a physical model of PCCI combustion to analyze the ignitability of the cylinder for each cycle. Ignitability controls the target Ignition Delay (ID) such that this determination can translate to cycle-by-cycle controls of ID. This control optimizes combustion and compensates for intake and transient engine conditions. This research developed a new PCCI control method to reduce the combustion noise level by changing ID based on ignitibility.

Jia et al. [25] studied the influence of the injection timing of a PCCI diesel engine on performance and emissions. It was found that PFI injection timing must be carefully timed in a PCCI combustion operating engine to best utilize the Intake Valve Closed (IVC) timing of an engine.

Shim et al. [18] studied HCCI, PCCI, and DF-PCCI in a heavy-duty single-cylinder engine. All these advanced combustion methods produced lower NOx and PM emissions compared to CDC. DF-PCCI was also seen to have a higher indicated thermal efficiency of 45.3% and reduced CO_2 emissions by 14.3%.

Partially Premixed Combustion Emissions Reduction

Belgiorno et al. [26] used a parametric analysis with a 2l Volvo Euro 6 diesel engine utilizing PPC. Using gasoline RON75 and MK1 diesel, it was determined that increasing the EGR from 0% to 30% provided an increase in efficiency by 1.5% due to the shortened combustion cycle. Soot levels in PPC were also seen to be two times lower than in diesel combustion. Combined with high levels of EGR and optimized pilot quantity, PPC was seen to have high efficiency without increasing NOx emissions.

Aronsson et al. [27] studied the Low Temperature Release (LTR) in HCCI and PPC using various different blends. These fuel blends include varying amounts of ethanol, n-heptane, iso-octane, and toluene. A Cooperative Fuel Research engine was utilized for the HCCI experiments and a single-cylinder highspeed direct-injected diesel engine for PPC. It was found that by increasing the ethanol and toluene in specific blends, the LTR fraction increases in PPC and decreases in HCCI.

Walker et al. [28] studied dual-fuel PPC and single-fuel PPC in a single-cylinder diesel research engine using isobutanol, iso-octane, and jet JP-5. It was found that dual-fuel PPC reduced NOx and soot emissions while having a reduced effect on Unburnt Hydrocarbon (UHC) and CO.

Dimitrakopoulos et al. [29] studied PPC for better efficacy and reduced emissions on a light-duty Euro 6 2L diesel engine. It was found that speed- and load-based EGR increased the gas exchange efficiency. It was also seen that as EGR moves from the long route to the short route, NOx was increased while soot was decreased.

An et al. [30] studied HCCI and PPC in a single-cylinder AVL diesel engine using PRF70. Engine simulations were also completed using CONVERGETM. It was found that HO_2 formation was more likely to occur in LTR than in high temperature release. Additionally, in both LTC methods soot and NOx formation were avoided.

Mao et al. [31] studied PPC in a six-cylinder common rail HD diesel engine using different EGR operating conditions. The fuel blends used in this experiment were composed of n-heptane, gasoline, and n-butanol and compared to a baseline of diesel. Each fuel blend was made with diesel by a volume ratio of 80%, denoted by DH80, DG80, and DG80. DH80 had the most effect on soot reduction when compared to diesel. Additionally, as the cetane number (CN) was reduced, a correlation was found with lower soot emissions.

Zheng et al. [32] studied PPC in a single-cylinder engine with n-butanol. The results found that n-butanol PPC is sensitive to high levels of EGR and intake pressure, resulting in poor controllability; however, THC, NOx, and soot were reduced. The combustion controllability could be improved using two-stage injection and increasing intake pressure.

Bio-alcohols

Stein et al. [33] studied the use of E85 in a turbocharged DI engine. It was found that E85 when used in higher load applications reduced knock. Additionally, at higher injection rates or colder temperatures, E85 was found to reduce engine oil longevity and increased wear. It was also found that when E85 was used, less DEF fluid was needed to keep NOx emissions lower.

Liang et al. [34] studied the environmental impacts with respect to emissions and power of neat Ultra Low Sulfur Diesel (ULSD)#2 and blends of biodiesel and n-butanol additive using a type SD080 diesel generator. It was found that when mixing n-butanol with other fuels such as diesel and biodiesel, NOx and soot emissions are reduced when compared to blends of diesel and biodiesel. n-Butanol also decreases soot particle size due to increased oxygen gas (O_2) .

Gainey et al. [35] studied the autoignition process of methanol, ethanol, n-propanol, isopropanol, n-butanol, isobutanol, and sec-butanol using an HCCI in a single-cylinder light-duty research engine. It was found that when boosted, n-butanol had an increased ITHR and, when mixed with other alcohols, shows minimal effect in autoignition properties.

Lopez et al. [36] studied hydrous ethanol and n-butanol fumigation in a 4-cylinder, 2.5L, turbocharged DI diesel engine. The results showed that when compared to ULSD and independent of engine load, both alcohols have higher

premixed combustion peaks and higher coefficients of IMEP. Both alcohols were seen to have increased CO and THC and reduced NOx and PM.

Rokopoulos et al. [37] studied the effects of n-butanol or ethanol diesel fuel on a heavy-duty turbocharged diesel engine. The results showed that when utilizing n-butanol or ethanol, diesel blends had irregular cyclic variations. It was also seen that ethanol diesel blends produced less soot than that of n-butanol.

Lapuerta et al. [38] studied the autoignition of biodiesel blends in a Constant Volume Combustion Chamber (CVCC). It was found that an increase in ethanol or butanol in the blends corresponded to a nonlinear increase in ID. As alcohol content was increased, the maximum pressure of combustion was decreased.

Rochon et al. [39] studied butanol and ethanol production through gas stripping-pervaporation from fermented sugarcane and sweet sorghum. The energy consumption of this Isopropanol, Butanol, and Ethanol (IBE) process was estimated through experimental data and different kinetic parameters. It was found that IBE production, when compared to butanol production by ABE fermentation, consumed less energy.

Calam et al. [40] studied HCCI in a single-cylinder SI-HCCI test engine using blends of n-heptane with ethanol, methanol, fuel oil, butanol, isopropanol, and naphtha. The results showed that during HCCI, ethanol has a greater indicated thermal efficiency with a maximum IMEP of 5.71 bar at 800 rpm. Butanol was also found to have 25% lower CO and HC emissions when compared to ethanol.

The increased heat of vaporization and the resulting reduction in the NOx emissions of bioethanol make it a suitable replacement fuel for ICEs. High flame speed leads to complete combustion in PCCI modes.

Nibin et al. [41] researched the effects of a Port Fuel Injection (PFI) of bioethanol and DI of wheat germ oil. With the PCCI operation of bioethanol and wheat germ oil emissions and combustion characteristics improved for the blended fuels. Experiments were conducted at 10%, 20%, and 30% PFI of bioethanol. At 30% PFI of bioethanol, the maximum thermal efficiency was shown to increase by 29.14% compared to that of diesel at 29.78%. NO emissions decreased from 813 ppm to 756 ppm and smoke emissions increased from 65% opacity to 78% opacity when comparing CDC to 30% PFI of bioethanol and 60% DI of wheat germ oil in PCCI. The introduction of bioethanol in PCCI decreased the ID and CD. CO and HC emissions were reduced with the addition of bioethanol in PCCI when compared to neat wheat germ oil.

Much research have been done on the use of biofuel blends in LTC methods for the reduction of emissions. In the direct comparison of the neat bio-alcohols n-butanol and ethanol, there is a large gap in research conducted with these fuels compared to CDC. This is important for providing an additional viable path for the reduction of emissions in ICEs with only the addition of one alternative fuel.

Economic Viability of Ethanol/ n-Butanol with Diesel

The economic viability of the use of each of these fuels is influenced by the source of the feedstock for production and the cost of fuel refinement from that feedstock. n-Butanol is an oxygenate derived from non-food biomass and agricultural waste in addition to the feedstocks used to create ethanol (starch- and sugar-based stocks) (ethanol feedstocks). Cellulosic ethanol can be also produced from non-food-based sources such as crop residues, lumber residue, and dedicated energy crops. In an evaluation by Aui et al., the cost per gallon of ethanol fuel based on the feedstock source is as follows: $$2.83 \pm 1.14$ /gallon from agricultural residue, $$2.70 \pm 0.76$ / gallon for woody biomass, and \$1.98 ± 1.02/gallon from grasses. Since ethanol is already a widely used fuel in spark ignition engines, there is less cost associated with the fuel refinery infrastructure necessary for production. With the need to produce more dedicated refineries, the estimated cost of n-butanol is estimated to be \$4.28/gallon compared to an average of \$2.50/gallon for ethanol. As the infrastructure is built alongside pathways for viable feedstocks, n-butanol will continue to decrease in price [42, 43, 44].

Experimental Methods

Preliminary Fuel Analysis Methods and Apparatuses

Multiple investigations were conducted on the thermophysical properties of ULSD#2, n-butanol, and ethanol (denoted as E98) to gain insight into their effect on combustion/emissions for PPC. The low temperature oxidation, thermal stability, spray development, viscosity, and Lower Heating Value (LHV) properties of the fuels were investigated. The thermophysical properties of ULSD, n-butanol, and ethanol that were important for PPC operation are displayed in Table A.1. Additional values that were not measured using in-house equipment but are important to engine operation are gathered from a literature review and are also presented in Table A.1. An investigation with a PAC CID 510 CVCC was attempted for measuring the Derived Cetane Number (DCN) of ethanol at a concentration of 98% but was deemed inconclusive as ethanol was unable to ignite due to its low reactivity. However, it was observed that E98 had some properties that were favorable for operation in a Compression Ignition (CI) engine for PPC such as its lower reactivity and higher oxygen content when compared to n-butanol.

One of the primary differences between ethanol and n-butanol is the ability to blend with ULSD. Ethanol cannot blend with ULSD without the use of an emulsifier while n-butanol has no issues with fuel separation. PFI of both fuels avoids the problems associated with fuel blends. The primary

TABLE 1 Physiochemical properties of ethanol and n-butanol. Data taken from Refs. [48, 49, 50].

Property	Butanol	Ethanol
Chemical formula	C ₄ H ₉ OH	C ₂ H ₅ OH
Molecular weight [g/mol]	74.12	46.07
Oxygen [%wt]	21.59	34.73
Density [kg/m³]	809.7	789.4
Boiling point [°C]	117	79
Autoignition temperature [°C]	345	366
Lower heating value [MJ/kg]	33.1	26.8
Latent heat of vaporization [kJ/kg]	585.4	918.42
Cetane number	25	8

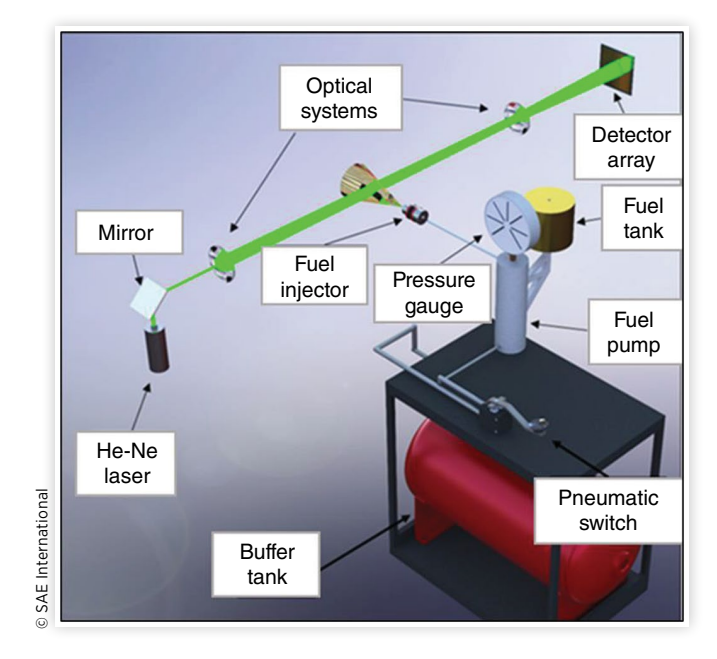
properties which affect the performance of the fuel in this experimentation are the density, autoignition temperature, LHV, and CN. Ethanol has a lower CN, density, and LHV, indicating that the fuel is likely to have a greater effect on the autoignition quality of the in-cylinder fuel mixture, but reduce efficiency. As ethanol and n-butanol are neat, the boiling point remains the same through all stages of vaporization. Since ethanol has a lower boiling point, the rate at which the fuel vaporized is much faster than n-butanol as represented by the Thermogravimetric Analysis (TGA) in the article. The physicochemical properties of ethanol and n-butanol are shown in Table 1.

Mie-Scattering Fuel Spray Apparatus

The spray droplet size distribution and mixture formation were determined for each of the researched fuels using a 632 nm wavelength Malvern He-Ne laser. The research apparatus, shown in Figure 1, allows a detailed investigation of the spray development from a single-hole pintle-type witness fuel injector. The fuel injection pressure was set at a constant 180 bar for each spray, and the injection was actuated with the injector nozzle tip positioned 100 mm away from and perpendicular to the laser beam. A detector array composed of 34 light-gathering sensors was located behind the datacollecting lens on the receiving side of the system. This array measures the angles of laser light diffraction caused by the introduction of the fuel spray into the beam. As was observed in previous studies by Soloiu et al. and Hwang et al. in CVCC research and Tsuji et al.'s investigation on the viscosities of biofuels, fuels with a higher viscosity tend to have an increased droplet size and can be correlated to a decrease in efficiency [51, 52, 53].

Fraunhofer diffraction and Mie-scattering theories were used to calculate the droplet diameter in flight based on the angle of diffraction. The scattering intensity of unpolarized laser light by a single spherical particle can be mathematically described by <u>Equation 1</u>. Where m represents the refractive

FIGURE 1 Malvern Mie-scattering He-Ne laser apparatus.



index of a particle, θ is the scattering angle of the light, and $x = \frac{\pi D}{\lambda}$, with D representing the particle diameter and λ representing the wavelength of the light coming from the laser. Furthermore, k is the wavenumber $2\pi/\lambda$, r is the distance from the scatterer to the detector, and S_1 and S_2 are dimensionless, complex functions describing the change of amplitude in the perpendicular and the parallel polarized light.

$$I_s(m,x,\theta) = \frac{I_0}{2k^2r^2} (|S_2|^2 + |S_1|^2)$$
 Eq. (1)

This Data Acquisition System (DAQ) interprets the signals from the detectors at a rate of 10 kHz with data recording occurring from 0.1 ms before injection to 5 ms after injection. The spray development is measured for 50 total data points with an accuracy of ± 0.5 (μm).

Fired Engine Experimental Apparatus and Methods

An experimental single-cylinder CRDI was utilized for conducting the investigation on PPC with either ethanol or n-butanol as the homogeneous air/fuel charge. The engine specifications can be found in <u>Table 2</u>, and the valve/injection timing can be seen in <u>Figure 2</u>. The engine has been outfitted with a PFI system as seen in <u>Figure 3</u>; the engine and subsequent fuel injection systems specifications can be seen in <u>Table 2</u> as well. An Omron 3600 ppr optical rotary encoder was attached to the crankshaft of the engine and utilized for rotational position tracking and engine speed. The encoder collected data every 0.18 crank angle degree (CAD), or every

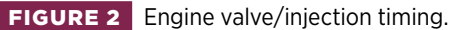
TABLE 2 Engine specifications.

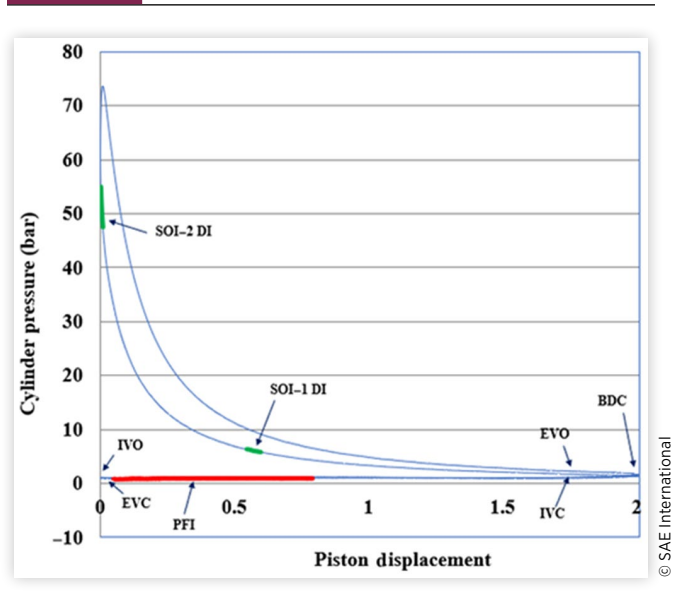
Peak power	17 kW at 2200 rpm
Peak torque	77.5 Nm at 1400 rpm
Bore × stroke	112 mm × 115 mm
Displacement	1.1L
Compression ratio	16:1
Piston geometry	Omega bowl in piston
Piezo DI nozzle	7 orifices × 0.115 mm
Bosch CRDI	800 bar in CDC; 600 bar in PPC
Cooling system	Water
Valves per cylinder	2
PFI pressure	2.8 bar
PFI timing	20 CAD (after intake starts)

22 ms, and was utilized by a National Instruments (NI) CompactRIO 9076 Drivven ECU for various real-time measurements of engine parameters. Modules 9751 (DI driver) and 9758 (PFI driver) were used to control the engine injection timing/duration, common rail pressure, PFI % by mass, and engine speed to achieve the desired combustion strategy and operating parameters for this investigation.

Emissions were measured for 2250 engine cycles at a sampling rate of 1 Hz, gaseous emissions (NOx, THC, CO, formaldehyde, and CO₂) were measured with an MKS 2030, 21 gas species Fourier Transform Infrared (FTIR) emissions analyzer, and soot emissions were measured in real time, with an AVL Model 483 Micro Soot Sensor. Both devices had their sampling lines maintained at 191°C to ensure no carbon buildup or condensation occurred.

A Yokogawa DL850 high-speed DAQ was used to record and monitor data from a Kistler 6053cc piezoelectric pressure transducer (in-cylinder pressure) with a 5010B dual-mode





amplifier, a Kulite pressure sensor (intake pressure), and an Omron 3600 ppr optical rotary encoder (engine rotational position and speed). The data collected per test are then averaged over 125 pressure cycles for post-processing and data analysis.

An AVL IndiCom utilized the same data channels for real-time monitoring of engine combustion characteristics such as in-cylinder pressure, Pressure Rise Rate (PRR), Coefficient of variability (COV), CA50, and Apparent Heat Release Rate (AHRR).

An NI DAQ was used to measure the fuel mass flow rate utilizing a 213 Max Flow Meter for the CRDI system and a P001 Max Flow Meter for the PFI system.

The sampling rate for both fuel flow meters were 1.25 MS/s, when using the NI DAQ for measurement recording. The measurement accuracies for the equipment utilized in the experimental apparatus can be seen in <u>Table 3</u>.

An uncertainty analysis was conducted using the accuracy/standard error of the equipment in <u>Table 3</u> along with the experimental setup of the equipment. These uncertainties exist from the environment and experimental approach and due to the varying accuracy ranges of the equipment, thus differing the nominal measured values. The root sum square method used includes two parameters, *xi* and *y*, where *xi* is the measured variable and *y* is the calculated parameter. The uncertainties determined for NOx, CO, formaldehydes, UHC, and soot are found in <u>Table 4</u>.

Uncertainty
$$(\%) = 100\% * \sqrt{\sum_{i=1}^{n} \left[\frac{dy}{dxi} * xi \right]^{2}}$$
 Eq. (2)

Fired Engine Experimental Methods

An investigation was conducted on the effects PFI of n-butanol or ethanol would have on PPC and emissions characteristics compared to CDC.

This investigation was conducted at a load of 4 bar and 5 bar IMEP with a CA50 set at 9° After Top Dead Center (ATDC), at a speed of 1500 rpm, ULSD was used as the DI fuel for all five combustion experiments conducted per load.

CDC was operated with only injection (SOI-2) at a common rail pressure of 800 bar, PPC experiments with either n-butanol or ethanol were conducted with both PFI fuel mass percentages of 30% and 40% and had common rail pressure set at 600 bar with a pilot injection at 60°BTDC with a pulse width of 0.35 ms.

Table A.2, located in the Appendix, contains the injection timing for each test conducted at loads of 4 bar and 5 bar IMEP. The naming scheme for PPC test points was named after the PFI % by mass followed by a two-letter initial for the bio-alcohol used for the given point. For example, PPC 30BU is for PPC conducted at a PFI % of 30% with n-butanol as the PFI fuel.

FIGURE 3 Fired engine experimental setup.

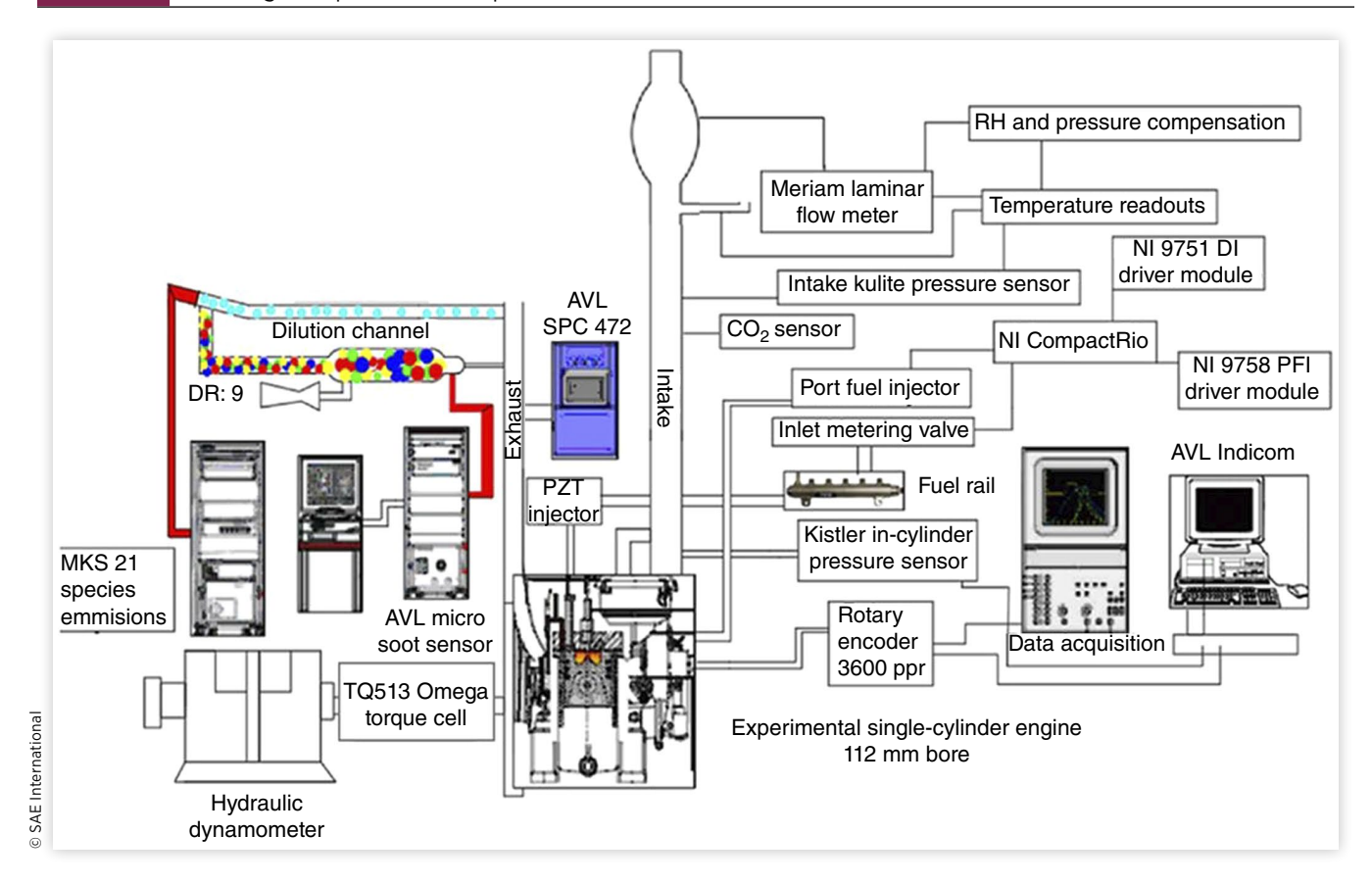


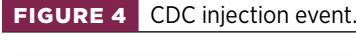
TABLE 3 Experimental apparatus measurement accuracies

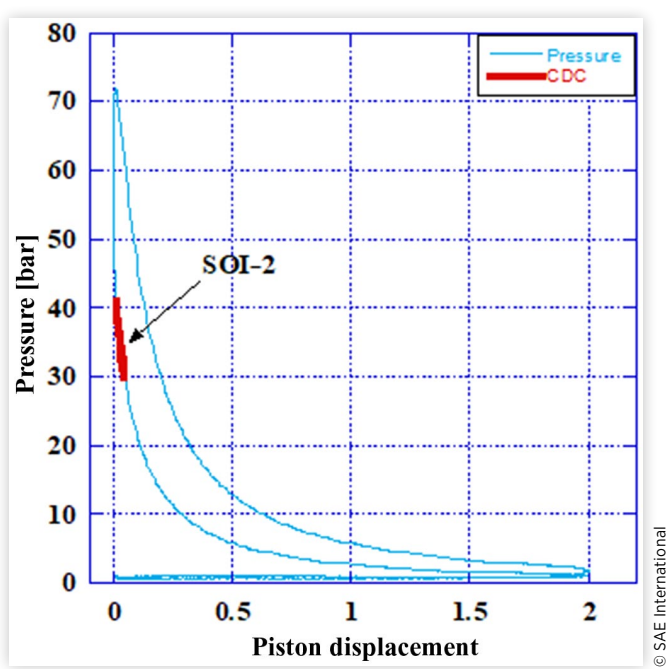
Instrument	Measured parameter	Accuracy
TQ513 Torque Sensor	Torque	±0.06%
Meriam Z50MC2-2 Laminar Flow Meter	Air mass flow rate	±0.72%
213 Max Flow Meter	Common rail fuel flow rate	±0.2%
P001 Max Flow Meter	PFI fuel flow rate	±0.2%
Kulite-175-190 M Intake Pressure Transducer	Intake pressure	±0.1%
Kistler 6053cc Piezoelectric Pressure Transducer	In-cylinder pressure	±0.19%
AVL 483 Micro Soot Sensor	Soot concentration	±3.8%
MKS FTIR 2030	NOx concentration	±2.0% of PPM auto range
	UHC concentration	
	CO concentration	
	CO ₂ concentration	
	Formaldehyde	
	concentration	

TABLE 4 Calculated uncertainties.

NOx	Soot	СО	Formaldehydes	UHC
2.72%	2.81%	2.85%	2.68%	3.20%

© SAE International





In <u>Figures 4</u> to <u>6</u>, indicated diagrams are shown with the pilot and secondary injection events overlayed for the five combustion events conducted at a load of 5 bar IMEP.

The injection timing for all experiments was selected for maintaining CA50 at 9 (±2 CAD ATDC, COV below 5%, the resulting global lambda from the chosen injection strategy at each load per test can be found in <u>Table 5</u>.

FIGURE 5 PFI, pilot and secondary injection events at 5 bar IMEP and n-butanol PFI.

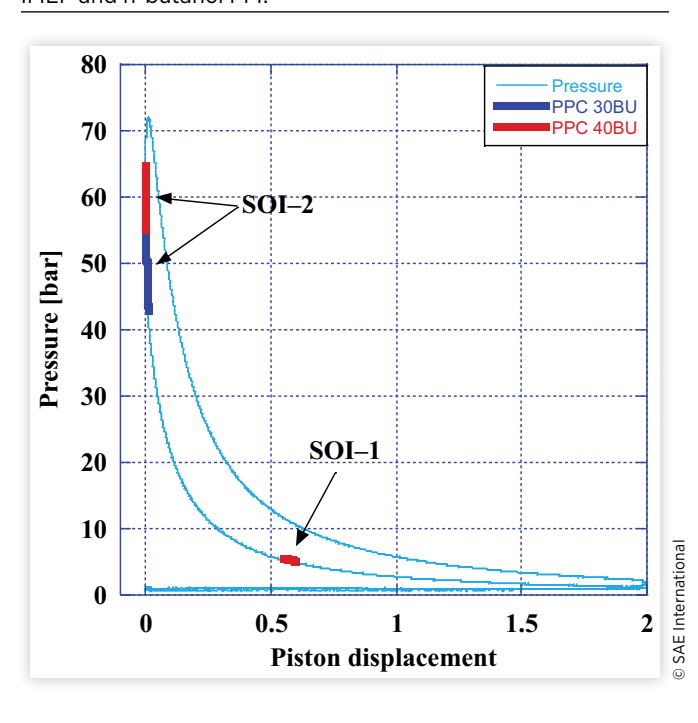
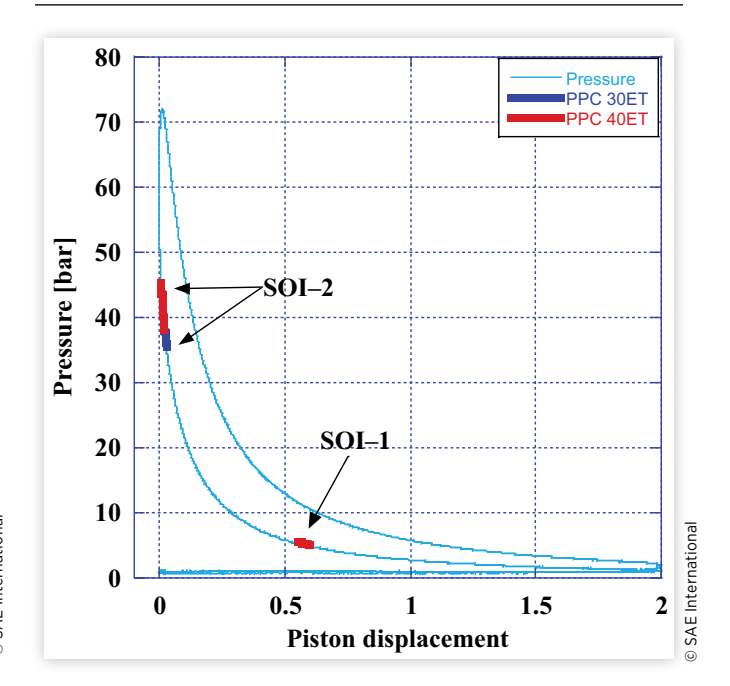


FIGURE 6 PFI, pilot and secondary injection events at 5 bar IMEP and ethanol PFI.



Data Reduction of Thermodynamic Equations

A data reduction analysis has been performed for the AHRR, RI, heat flux, and Reynolds number for further understanding of important parameters of this study.

$$\Delta U = Q - W$$
 Eq. (3)

The first law of thermodynamic is used in this article to calculate both the Ringing Intensity (RI) and the AHRR produced from combustion. By using this principle, thermal losses in the system can be accounted for to accurately determine the AHRR. The equation for this law, shown above, is used to derive the equation used to calculate AHRR.

The equation for AHRR is shown in <u>Equation 4</u> where the result of the equation is the heat release rate which is isolated at the change in heat divided by the change in CAD. Pressure and volume are represented on the right side of the

TABLE 5 Global lambda.

4 bar IMEP		5 bar IMEP	
Test point	Global lambda	Test point	Global lambda
CDC	4.26	CDC	3.26
PPC 30BU	3.76	PPC 30BU	3.18
PPC 30ET	4.01	PPC 30ET	3.19
PPC 40BU	3.85	PPC 40BU	3.36
PPC 40ET	3.98	PPC 40ET	3.32

© SAE International

equation additionally taken in terms of CAD. The constant γ representing the ratio of the specific heats.

$$\frac{dQ}{d\theta} = \frac{1}{[\gamma - 1]} V \frac{dP}{d\theta} + \frac{\gamma}{[\gamma - 1]} P \frac{dV}{d\theta}$$
 Eq. (4)

The RI calculation follows the first law as well, using only the change in pressure and maximum temperature to calculate the final value. The constants used in the equation are γ , β , and R, where R is the ideal gas constant, γ ratio of the specific heats, and β is the relationship between pressure pulsation amplitude and maximum PRR. In this study, the Peak Pressure Rise Rate (PPRR) of the engine is not representative of knock at all loads; thus, the RI correlation containing β was used; it is defined as 0.05. This value was devised by Dec et al. through their analysis of pressure waves while investigating HCCI combustion techniques [54, 55, 67].

$$RI = \frac{\left(\beta \left(\frac{dP}{dt}\right)_{max}\right)^{2}}{\left(2\gamma P_{max}\right)} \sqrt{\gamma RT_{max}}$$
 Eq. (5)

Alongside the determinations for AHRR, heat losses were calculated using the same base principles as it is a significant contribution to the reduction in fuel efficiency. These heat losses are localized to thermal boundaries where the hot gases from combustion change temperature, the largest of which occurs at the cylinder walls. The models used for the calculation of heat loss and heat flux are based on a study by Borman and Nishiwaki and further refined by Soloiu et al. [56, 57].

$$\dot{q} = A \frac{\lambda_A}{D} R e^{0.7} \left(T_A(\alpha) - T_W \right) + \sigma * \varepsilon \left(T_A^4(\alpha) - T_W^4 \right) \quad \text{Eq. (6)}$$

The model assumes a uniform wall temperature (T_W) , an in-cylinder Reynolds number (Re), and the air thermal conductivity (λ_A) function of crank angle.

The convection heat flux mapping used a revised model from Annand and Ma and further developed by Nishiwaki and Soloiu. This model effects areas where combustion gas comes in contact with the walls of the cylinder, piston crown, and cylinder head.

Flame and spray interactions are the primary determiners of the movement of heat as the majority of combustion heat transfer is due to convection heat transfer. This is especially true in LTC strategies as these methods decrease the diffusion phase for a reduction in soot.

Radiation heat transfer is generated from soot particles as the heat causes them to luminesce. This is assumed to be black-body radiation and is modeled using the Stefan-Boltzmann model which is the second term of Equation 6 [58].

Reynolds number is calculated using the equation below. Density and viscosity are represented as $\rho(\alpha)$ and $\mu(\alpha)$ function of crank angle, respectively. These values were determined for the combustion gases every 0.18 CAD. The other three values

in the equation are *N*, *S*, and *D* representing engine speed, stroke, and bore, respectively.

$$Re(\alpha) = \rho(\alpha) \frac{S * N * D}{30\mu(\alpha)}$$
 Eq. (7)

Results and Discussion

Low Temperature Oxidation and Thermal Stability Analysis

The TGA measures the volatility of the researched fuels by recording the change in mass of the sample in the cell environment of increasing temperature. As seen in Figure 7, E98 loses mass at a higher rate than both ULSD and n-butanol; this indicates that E98, when injected, would create a more homogeneous air/fuel mixture due to its higher volatility.

In <u>Table 6</u> the temperature at which 10%, 50%, and 90% of the fuel mass were vaporized can be found, denoted by TA(10), TA(50), and TA(90), respectively. The extreme volatility of E98 is apparent as the TA(90) of the fuel is approximately 18°C lower than n-butanol. This indicates that E98, when compared to n-butanol, more readily vaporizes when port fuel injected into the intake manifold of the engine, creating a more homogeneous air/fuel mixture. While ULSD

FIGURE 7 TGA.

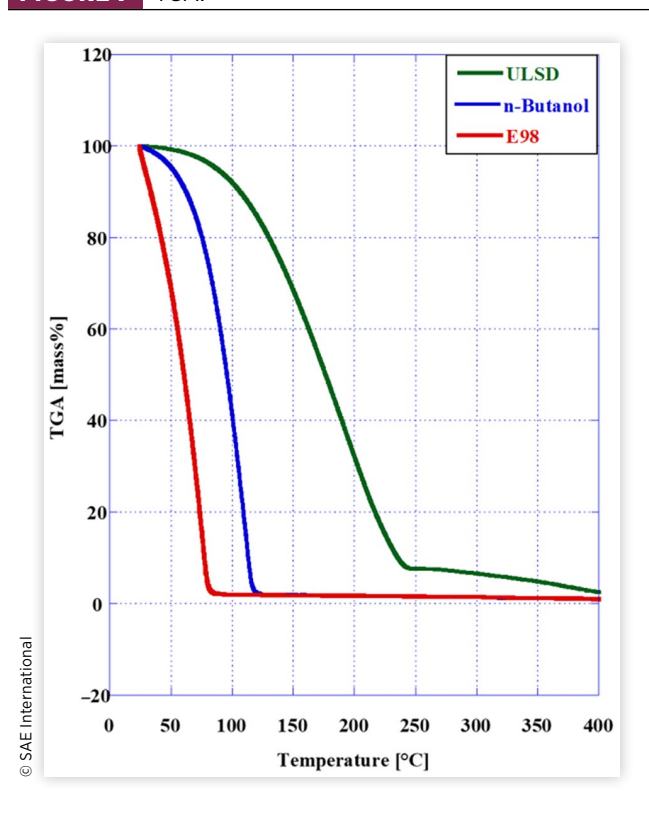


TABLE 6 Volatility of researched fuels.

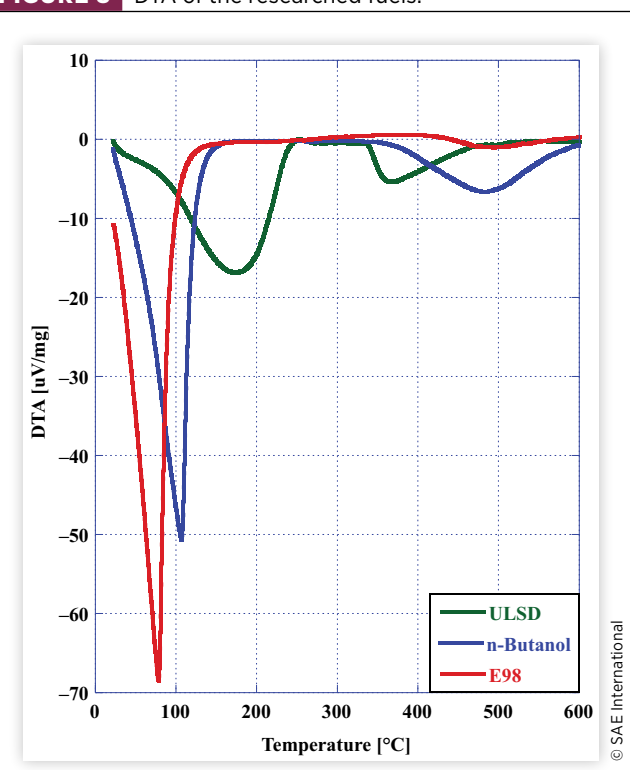
		n-Butanol		-
TA%	ULSD [°C]	[°C]	E98 [°C]	5
TA(10)	110.0	54.3	33.4	le noite anotal
TA(50)	180.0	80.8	60.6	
TA(90)	240.0	95.4	77.3	0 C A E

has a TA(90) that is 32°C higher than E98, its volatility is inefficient for a PFI process.

The Differential Thermal Analysis (DTA) analysis, as seen in Figure 8, is a study of the endothermic during the fuel vaporization and exothermic reactions occurring during the low temperature oxidation of the sample fuel. The endothermic reaction was represented by the negative slope in the DTA curve while the positive slope represents the exothermic reactions. Through the experiment, as temperature increases, the endothermic reaction increases until no more energy can be absorbed by the sample and begins to oxidize. E98 has the steepest negative and positive slopes as well as the largest negative peak DTA, thus emphasizing its higher volatility compared to that of n-butanol and ULSD.

The greater endothermic reaction of E98 indicates that a greater drop in temperature would occur at the site of injection, further reducing manifold temperature and in-cylinder compression stroke temperature. This was confirmed during fired engine research as will be seen in the next sections.

FIGURE 8 DTA of the researched fuels.



Viscosity and LHV Analysis

As the temperature of the fuel increased, the shear stress between the water jacket and spindle was seen to decrease, thus resulting in a lower viscosity. <u>Figure 9</u> below shows the viscosity curve for the researched fuels with respect to temperature.

During the viscosity test, E98 was unable to reach 90°C due to the fuel completely vaporizing before the test could be concluded. As seen in <u>Table 7</u> below, ULSD was observed to have the highest viscosity of the research fuels with 2.52 cP at 40°C. n-Butanol had the second highest viscosity with 2.04 cP at 40°C, followed by E98 with 1.15 cP at 40°C.

The average LHV of the researched fuels can be seen in Table 8 below. USLD was found to have the highest LHV at 45.1 (MJ/kg), followed by n-butanol with 32.0 (MJ/kg) and E98 at 24.7 (MJ/kg). The lower energy content of both n-butanol and E98 indicates that greater fuel consumption may occur for PPC than CDC due to the increased fuel mass required for the same amount of work.

Mie-Scattering Fuel Spray Analysis

The spray analysis was conducted for ULSD#2, n-butanol, and ethanol, and the atomization characteristics of the three fuels

FIGURE 9 Viscosity measurements for the researched fuels.

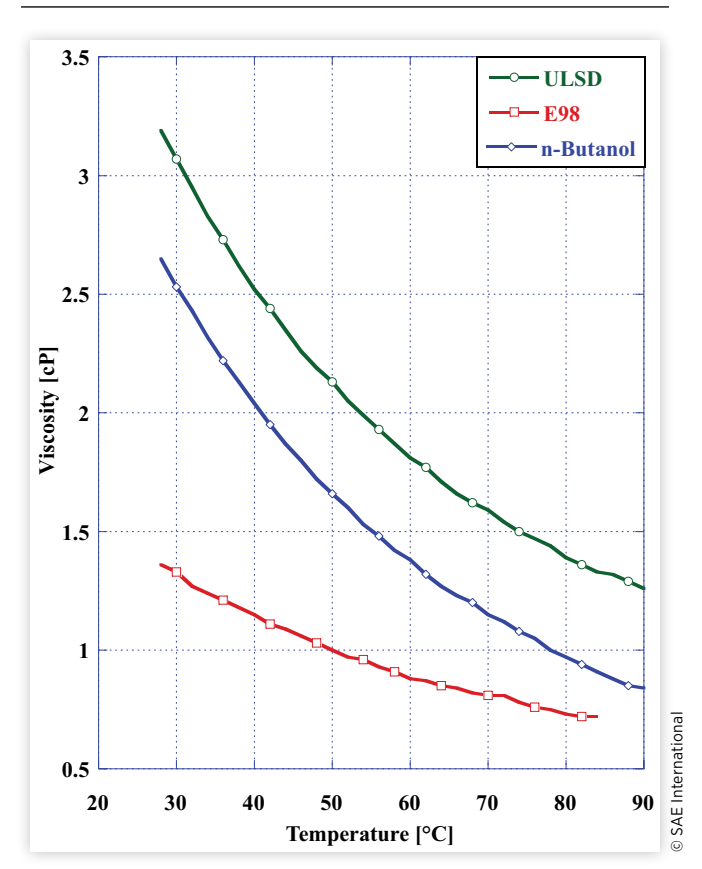


TABLE 7 Viscosity of the researched fuels at 40°C.

	ULSD	n-Butanol	E98
Viscosity at 40°C [cP]	2.52	2.04	1.15

© SAE International

TABLE 8 Calorimeter results.

Fuel	LHV [MJ/kg]
ULSD	45.1
n-Butanol	32.0
E98	24.7

© SAF International

were compared against each other. n-Butanol was found to have the smallest average Sauter Mean Diameter (SMD) over time compared to the other fuels. n-Butanol and ethanol have lower viscosity compared to ULSD, which correlated to smaller maximum droplet diameters measured than those of ULSD#2. The most frequently measured droplet diameter for n-butanol sprays was 30 μm , which consisted of 7.6% of the spray by volume. By comparison, 8.5% of the ethanol spray by volume was composed of droplets with a diameter of 30 μm . The spray volume percentiles based on droplet SMD are displayed in Table 9, and the results show that n-butanol has an average of 5 μm smaller SMD compared to ethanol for the same injection parameters.

DV (10) denotes the diameter that 10% of the spray droplets by volume are less than or equal in size. DV (50) is the corresponding diameter for 50% of the spray volume, and DV (90) denotes the same for 90% of the spray volume. The ethanol sprays exhibited a droplet size distribution that is noticeably more concentrated about the most frequent droplet diameter, whereas n-butanol and diesel droplets are more distributed over different ranges of diameters as seen in Figure 10. Ethanol does however still contain droplets that are larger than that of n-butanol for 90% of the spray volume. This may be explained due to the higher volatility of ethanol at room temperatures leading to smaller fuel droplets vaporizing prior to crossing the laser beam as was observed in the TGA.

Combustion Pressure

In-cylinder combustion pressure was measured for both PPC with either n-butanol or ethanol at PFI % by mass of 30% and 40% compared to CDC at loads of 4 bar and 5 bar IMEP (Figure 11).

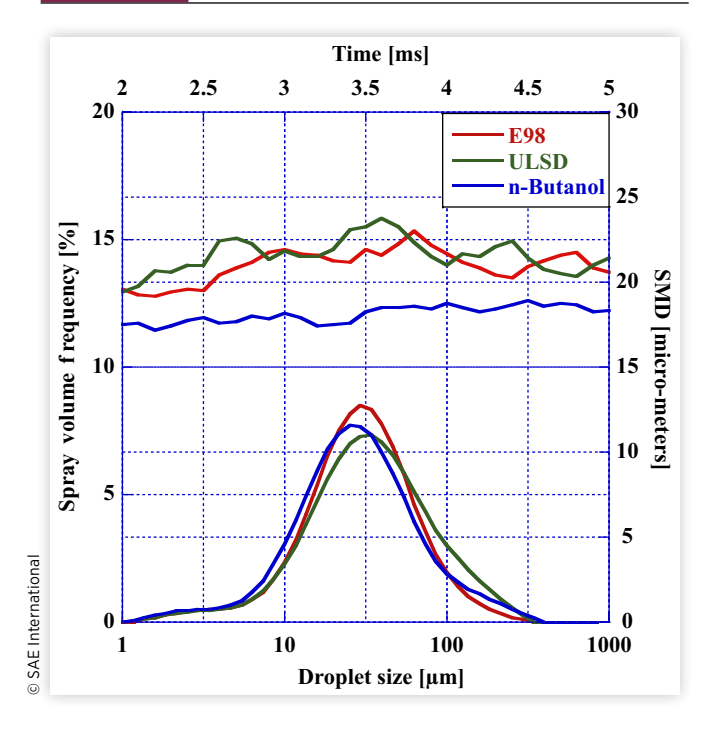
The motoring curve was included for reference, and the beginning of the cycle was set at the start of the intake stroke.

TABLE 9 Particle size distribution by volume (µm).

	ULSD	n-Butanol	E98
DV (10)	12.5	12.23	24.8
DV (50)	40.1	34.2	65.3
DV (90)	131.1	88.21	91.0

© SAE International

FIGURE 10 Spray SMD distribution and development.



In <u>Figure 12</u> it was observed that PPC with n-butanol had greater peak pressures than PPC with ethanol at both PFI rates at a load of 4 bar IMEP with PPC 40BU at 69.1 bar. It was shown that as PFI % increased from 30% to 40%, peak pressure increased in both PPC with n-butanol and ethanol, with n-butanol having a greater pressure than ethanol per PFI %. This is likely due to the slightly higher reactivity of n-butanol than ethanol in conjunction with the late CA50 of 9°ATDC

FIGURE 11 Combustion pressure at 4 bar IMEP.

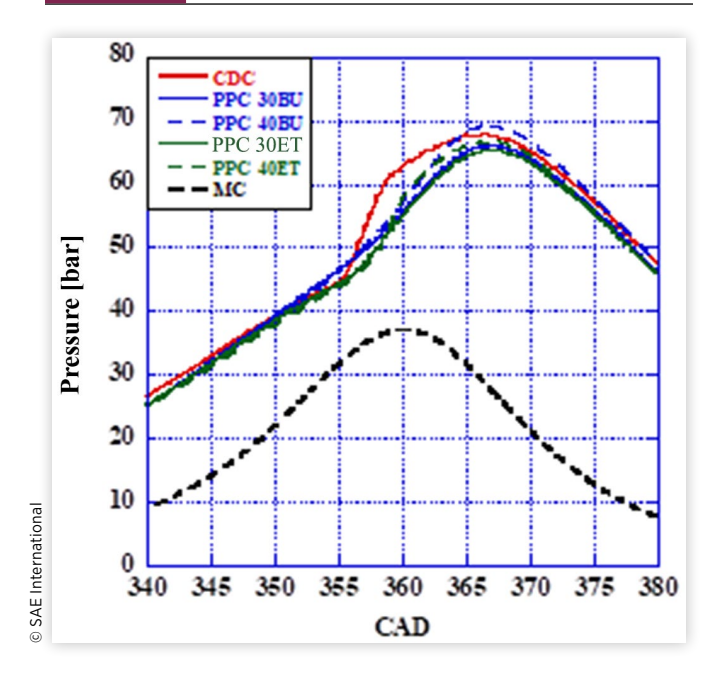
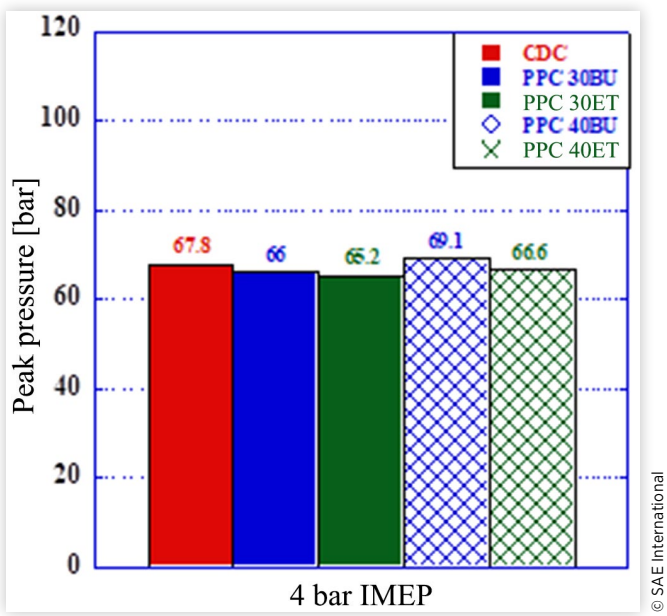


FIGURE 12 Maximum pressure at 4 bar IMEP.



used for this investigation causing n-butanol to combust more readily than ethanol, leading to the increase in peak pressure.

The location of peak pressure for each combustion test can be found Table 10, all the combustion experiments for 4 bar IMEP were located at 367 CAD ± 1 bar. Both CDC and PPC 40BU had the earliest peak pressures at 366.5 CAD out of all five combustion experiments, with PPC 40ET having the latest at 367.6 CAD.

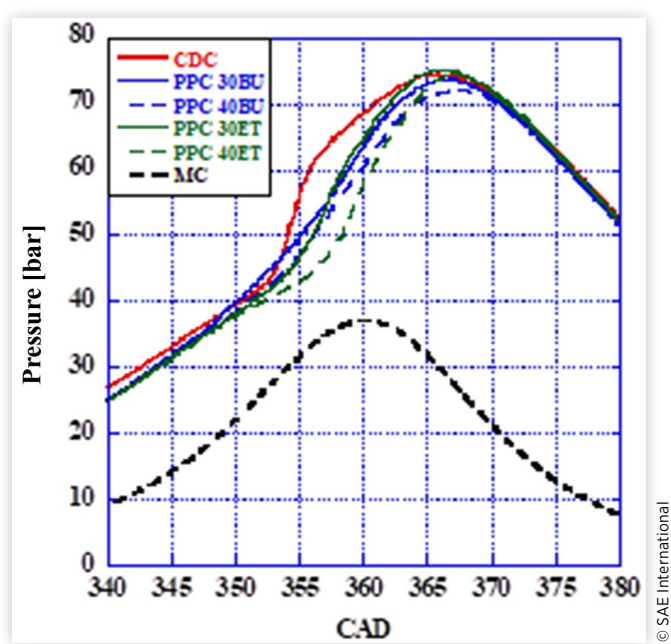
Figure 13 contains the pressure traces for all five combustion experiments conducted at a load of 5 bar IMEP where it can be observed that PPC with n-butanol had the lowest peak pressure of all five experiments for both 30% and 40% PFI. This occurred contrary to the behavior observed at a lower load of 4 bar IMEP where PPC with n-butanol had the greatest pressure. At the higher load of 5 bar IMEP, PPC with ethanol at 30% PFI had the greatest peak pressure of 74.9 bar. For both PPC with either n-butanol or ethanol, peak pressure was reduced with an increase in PFI % by mass utilized, as observed PPC with n-butanol experienced the greatest decrease by 1.7 bar (Figure 14).

The location of peak pressure for experiments conducted at 5 bar IMEP can be found in Table 11. It is observed that CDC had the earliest peak pressure at 365.9 CAD. All the PPC

TABLE 10 Peak pressure CAD at 4 bar.

Combustion test	Peak pressure location [CAD]	
CDC	366.5	_
PPC 30BU	367.0	Internationa
PPC 30ET	367.4	erna
PPC 40BU	366.5	
PPC 40ET	367.6	SAE

Combustion pressure at 5 bar IMEP.



peak pressures occurred at 367 CAD with a maximum deviation of +0.8 CAD, thus indicating PPC to have higher stability with increased loads utilizing either n-butanol or ethanol. This stability is attributed to the more desired combustion rate of the dual-fuel PPC method compared to that of CDC [32]. Even though there is larger in-cylinder fuel reactivity of the combustion produced by PPC, the peak pressures are lower that of ULSD CDC in 5 bar IMEP for all PPC experiments besides that of PPC 30ET. The combustion stability of the fuels will be analyzed further in the PRR and AHRR analysis.

FIGURE 14 Maximum pressure at 5 bar IMEP.

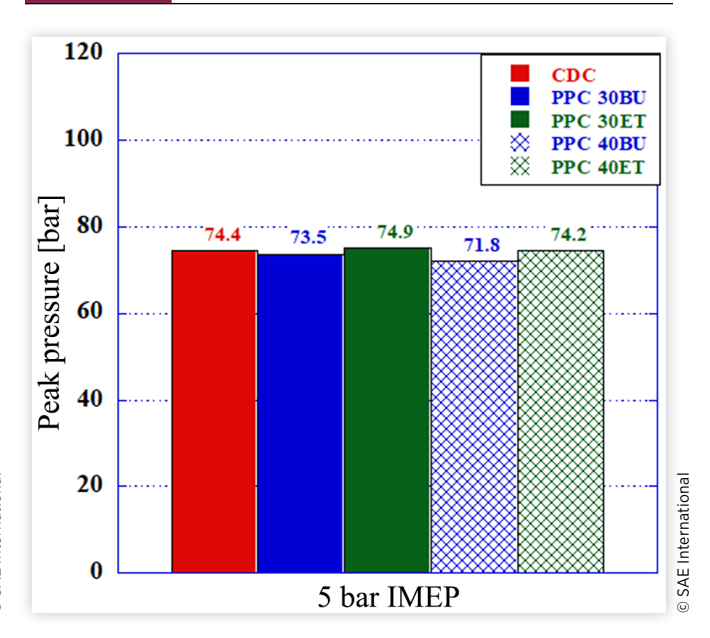


TABLE 11 Peak pressure CAD at 5 bar IMEP.

	Combustion test	Peak pressure location [CAD]
_	CDC	365.9
rnationa	PPC 30BU	367.0
ernat	PPC 30ET	367.8
E Inter	PPC 40BU	367.2
© SA	PPC 40ET	367.6

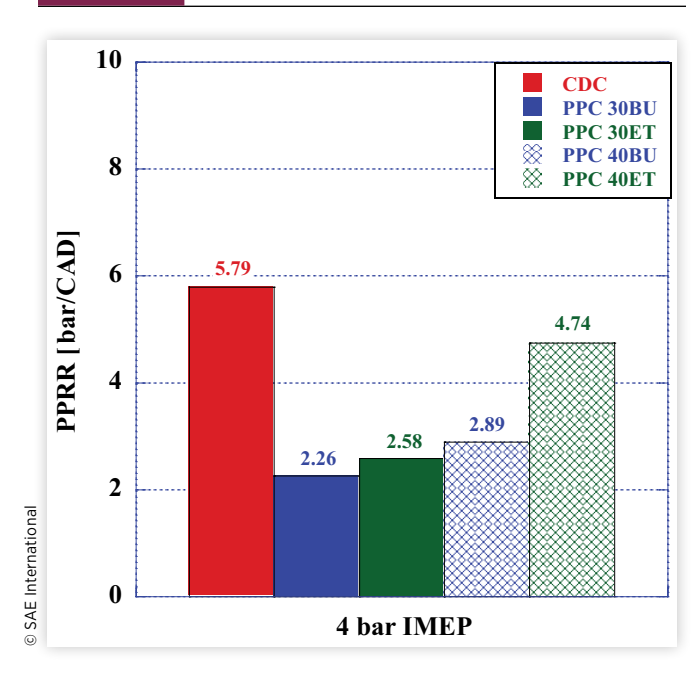
Pressure Rise Rate

PPC in previous investigations has been shown to reduce PRR as seen in Han et al. [59]. As is the case, the same observation can be seen in Figure 15 where all PPC experiments conducted at 4 bar IMEP have a reduced PPRR compared to CDC. PPC with n-butanol had the greatest reduction in PPRR compared to ethanol for both 30% and 40% PFI. As PFI % was increased, PPRR was also increased for both fuels with ethanol having the greatest rise in PPRR of 2.16 bar/CAD in comparison to n-butanol with a rise in PPRR of only 0.63 bar/CAD (Figure 16).

The PRR for CDC at a load of 4 bar IMEP had the greatest PPRR of all the combustion experiments at this load and the shortest occurring PRR compared to PPC. All PPC experiments except for ethanol at PFI 40% had PRR occur over a broader area; PPC 40ET however experienced a PRR like CDC with a pronounced peak versus the other PPC broad PRR. The sharp PRR of PCC ET40 can be attributed to the poor combustion stability PPC exhibits under low loads [32]. As the load increased, the combustion during PPC is more stable and controllable.

In <u>Figure 17</u>, it is observed that a higher load PPRR is increased for all combustion experiments and affected PPC.

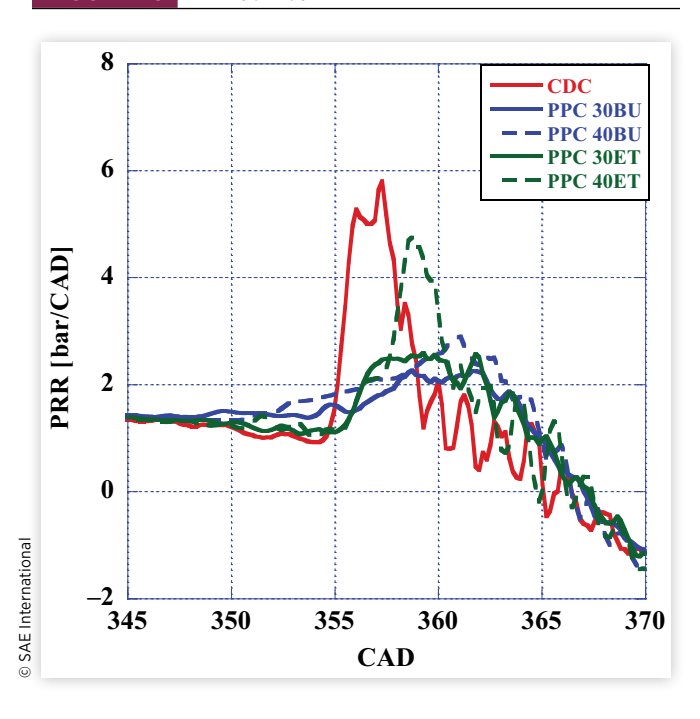
FIGURE 16 PPRR at 4 bar IMEP.



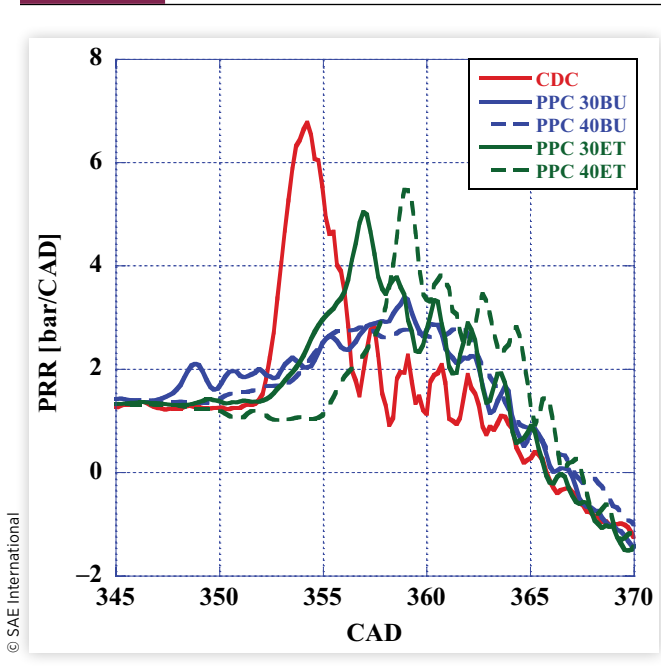
As such, n-butanol was shown to decrease PPRR with the increase in PFI %. Contrarily, PPC with ethanol had an increase in PPRR as PFI % was increased, but to a lesser extent than at 4 bar IMEP (Figure 18).

The PRR for all combustion experiments for 5 bar IMEP exhibited a sharper increase in PRR compared to 4 bar IMEP. PPC with n-butanol for both 30% and 40% PFI had the broadest increase in PRR of all five combustion experiments,

FIGURE 15 PRR at 4 bar IMEP.









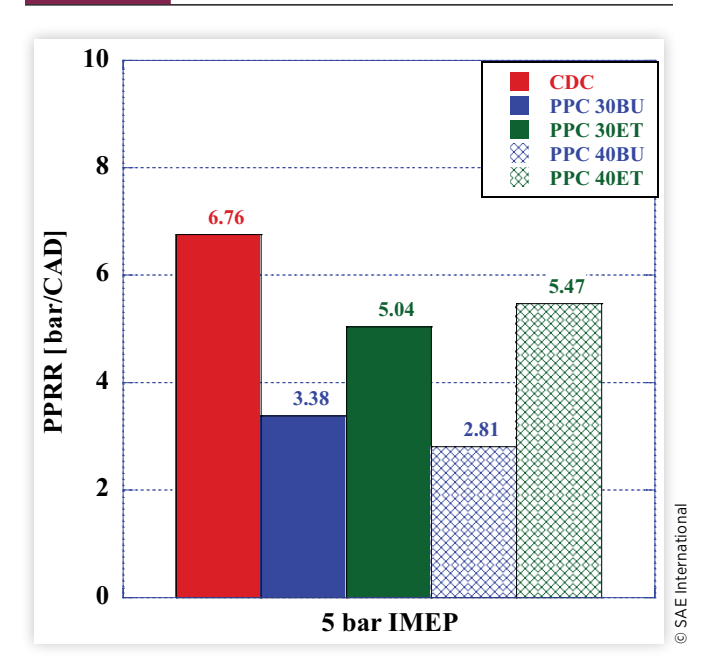
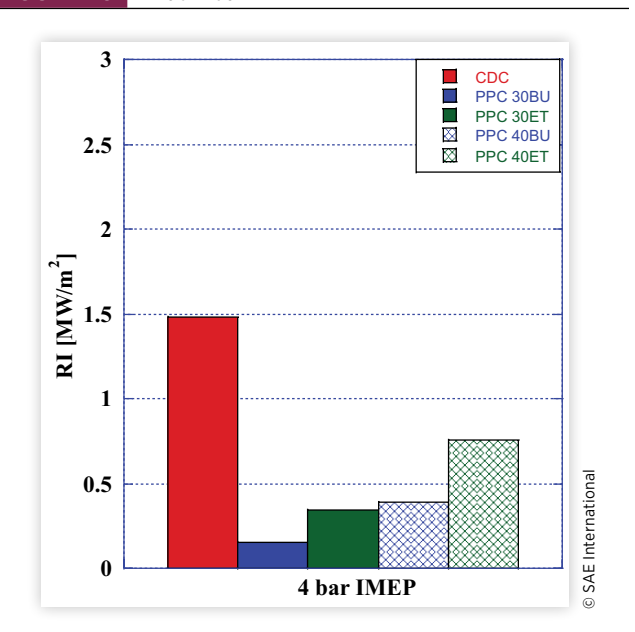


FIGURE 19 RI at 4 bar IMEP.



while PPC with ethanol exhibited a PRR similar to CDC where a sharp increase in PRR occurs.

Ringing Intensity

The RI for all five combustion experiments conducted at loads of 4 bar and 5 bar IMEP were calculated utilizing Equation 5 [51], using the PPRR, maximum temperature, and peak pressure of the averaged cycles. To protect the research engine and the sensors that have been implemented into it, the maximum limit value of RI is set to 2.5 MW/m².

RI =
$$\frac{\left(\beta \left(\frac{dP}{dt}\right)_{max}\right)^{2}}{\left(2\gamma P_{max}\right)} \sqrt{\gamma RT_{max}}$$
 Eq. (5)

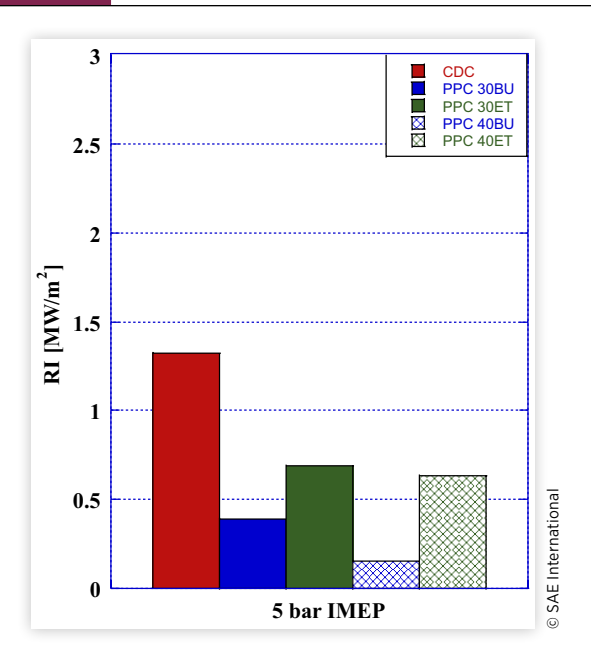
The RI for all combustion experiments conducted at 4 bar and 5 bar IMEP are shown in Figures 19 and 20, where it was observed that PPC had a lower RI than CDC. PPC with n-butanol was shown to have the greatest reduction in RI compared to CDC for both PFI 30% and 40% at a load of 4 bar IMEP. PPC 30BU had the lowest RI with a reduction of 84.76% compared to CDC. PPC with ethanol however only had an RI reduction of 76.62% compared to CDC at a PFI of 30%. PPC with ethanol as a result of its greater PPRR than n-butanol for both PFI 30% and 40%, resulting in its RI being higher than PPC with n-butanol despite its lower reactivity.

It was observed at 5 bar IMEP that as PFI % was increased for both PPC with ethanol or n-butanol, RI decreased contrary to the trend observed at 4 bar IMEP. PPC with n-butanol at a PFI of 40% had a RI reduction of 88.5% compared to CDC whereas PPC 40ET was only able to reduce RI by 51.74%

compared to CDC. As was the case for 4 bar IMEP, ethanol had a greater PPRR resulting in the increase in RI for a load of 5 bar IMEP.

As the load increased, RI was reduced with an increase in PFI % indicating the two have an inverse relation to each other with n-butanol having the greatest decrease in RI with the increase in PFI % at higher loads. This occurs despite n-butanol having a higher reactivity (16.4 DCN) than ethanol (8.0 DCN).

FIGURE 20 RI at 5 bar IMEP.



The increase in PPRR and RI could be attributed to possibly increasing the local lambda at the DI plume of ULSD PPC, which will also be discussed later.

ethanol having higher oxygen content than n-butanol, thus leading to a reduction of soot emissions (soot emissions will be discussed later in the manuscript). The larger by mass amounts of PFI fuel injected increases both PPRR and RI. These reactions occur despite the increased ID with ethanol

Apparent Heat Release Rate

The AHRR was calculated utilizing the first law of thermodynamics as shown in Equation 4; the system was treated as a closed system (after IVC and before EVO) with appropriate compensations made for the mass introduced from DI events and the mass lost from the system due to blowby as observed in [<u>60</u>].

$$\frac{dQ}{d\theta} = \frac{1}{[\gamma - 1]} V \frac{dP}{d\theta} + \frac{\gamma}{[\gamma - 1]} P \frac{d\nu}{d\theta}$$
 Eq. (4)

The AHRR for all combustion experiments conducted at a load of 4 bar IMEP can be found in Figure 21 with peak AHRR shown in Table 12. It was observed that CDC had the greatest peak AHRR compared to all PPC experiments conducted; however, all PPC experiments conducted had heat release occur for a greater length of time than CDC as a result of both High Temperature Heat Release (HTHR) and Low Temperature Heat Release (LTHR) occurring for a longer duration. PPC with ethanol at 40% PFI, however, had a peak AHRR comparable to that of CDC at 79.98 J/CAD compared to CDC peak AHRR at 89.42 J/CAD. However, all other PPC experiments conducted had a notable reduction in peak

TABLE 12 Peak AHRR at 4 bar IMEP.

	Combustion test	Peak AHRR [J/CAD]
	CDC	89.42
	PPC 30BU	51.59
ernai	PPC 30ET	53.45
SAE International	PPC 40BU	59.55
0	PPC 40ET	79.98

AHRR occur as PPC 40BU had only a peak AHRR of 59.55 J/ CAD with even further reductions occurring for both PPC experiments conducted at PFI of 30%.

Although PPC 40ET exhibited an HTHR event similar to CDC, it was observed that LTHR occurred for an extended period of time compared to CDC as did the other PPC experiments conducted. The LTHR for PPC with n-butanol at 30% and 40% PFI had two small LTHR events occur prior to the main LTHR event whereas PPC with ethanol only had the primary LTHR event occur; this is a result of the lower reactivity of ethanol as supported from previous studies on ethanol DCN [46]. As a result, PPC 30BU and PPC 40BU had LTHR occur prior to the secondary injection event as seen in Figure 22 due to the late injection strategy and the higher reactivity of n-butanol than that of ethanol. Due to the lower reactivity of ethanol than that of n-butanol, LTHR occurred after the second injection event, thus indicating a greater control for combustion at low loads despite the higher RI observed previously. This event comes at the cost of a reduced LTHR region and may lead to higher NOx emissions as more fuel is combusted during HTHR.

As was previously observed at a load of 4 bar IMEP, PPC with ethanol had an HTHR event similar to CDC at a load of 5 bar IMEP. This combustion characteristic of PPC with

FIGURE 21 AHRR at 4 bar IMEP.

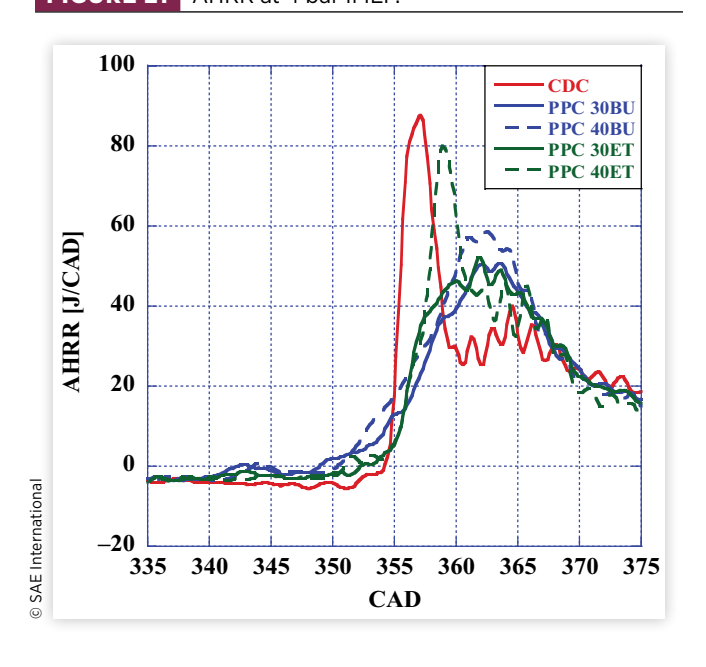


FIGURE 22 LTHR region at 4 bar IMEP.

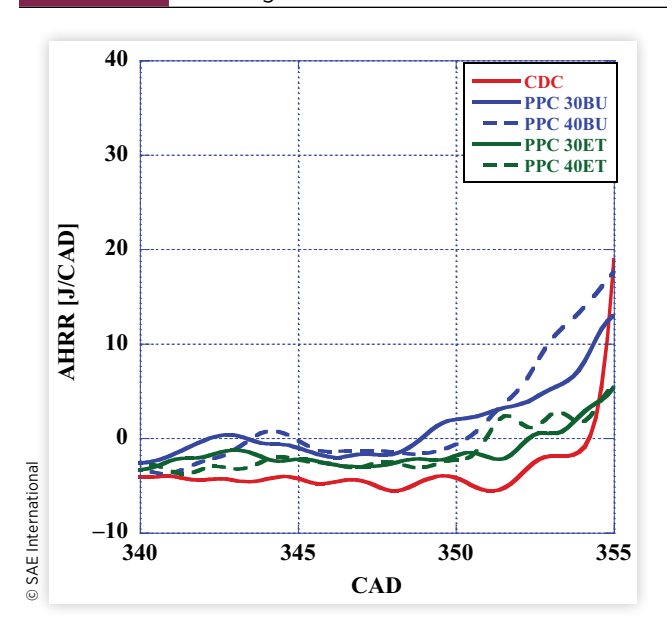


FIGURE 23 AHRR at 5 bar IMEP.

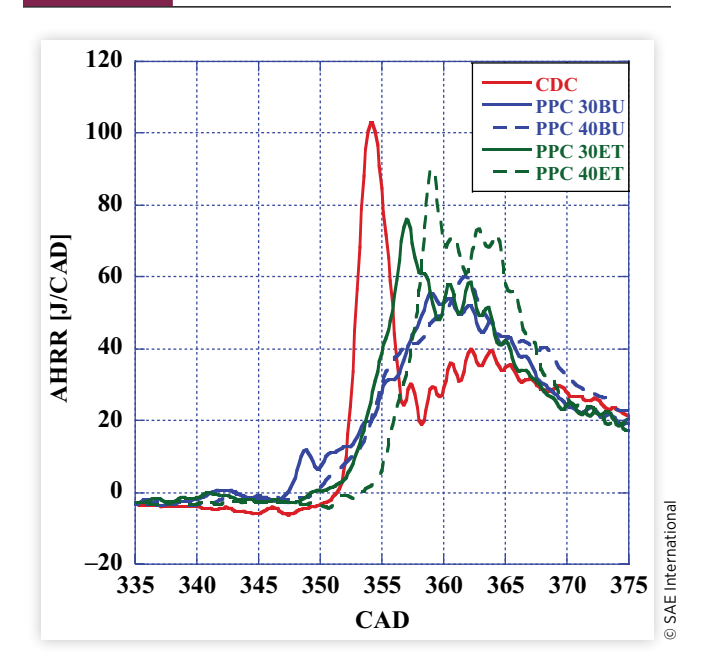
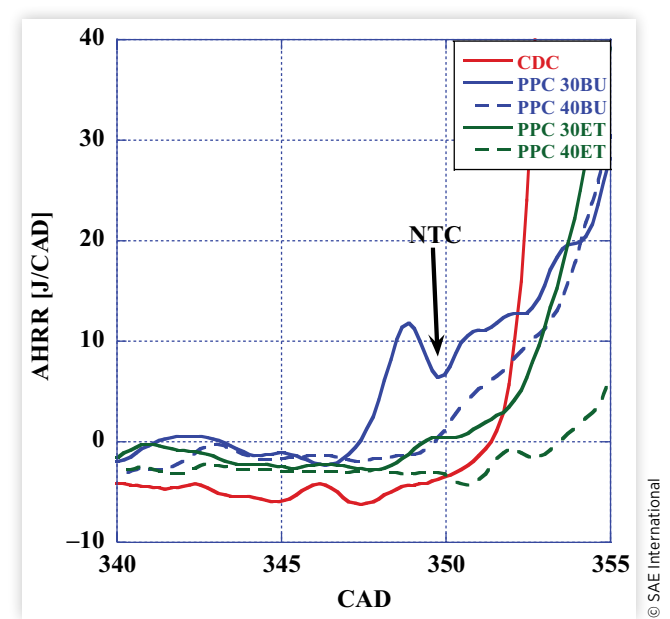


FIGURE 24 LTHR and NTCR regions at 5 bar IMEP.



ethanol leads to an increase in peak AHRR compared to PPC with n-butanol, as seen in <u>Figure 23</u> and <u>Table 13</u> where PPC 40ET reached a peak AHRR of 90.26 J/CAD whereas PPC 40BU was only at 60.19 J/CAD.

LTHR for CDC at 5 bar IMEP was nonexistent and only HTHR occurred while PPC 30BU was shown to have a small LTHR proceeded by the NTC event occurring prior to the main injection (Figure 24). Additionally, a small HTHR event occurs prior to the main injection event. This event was not observed in PPC 40BU, as only an HTHR event was observed, prior to the main injection.

This indicates that the primary combustion event was initiated from the pre-ignition of the n-butanol/ULSD homogeneous mixture indicating that premixed combustion was dominant rather than the diffusion combustion from the second injection of ULSD that occurred at 2 CAD BTDC. PPC with ethanol however had no heat release occur prior to the second injection event indicating a greater control for PPC with late injection strategies, PPC 30ET had an increased LTHR event compared to PPC 40ET which was mostly comprised of HTHR combustion like that of CDC.

A characteristic of PPC with DI between 12° and 6° BTDC is the dual peak or an extended AHRR. This is apparent in all

TABLE 13 Peak AHRR at 5 bar IMEP.

Combustion test	Peak AHRR [J/CAD]	
CDC	102.94	
PPC 30BU	55.35	
PPC 30ET	75.95	
PPC 40BU	60.19	
PPC 40ET	90.26	

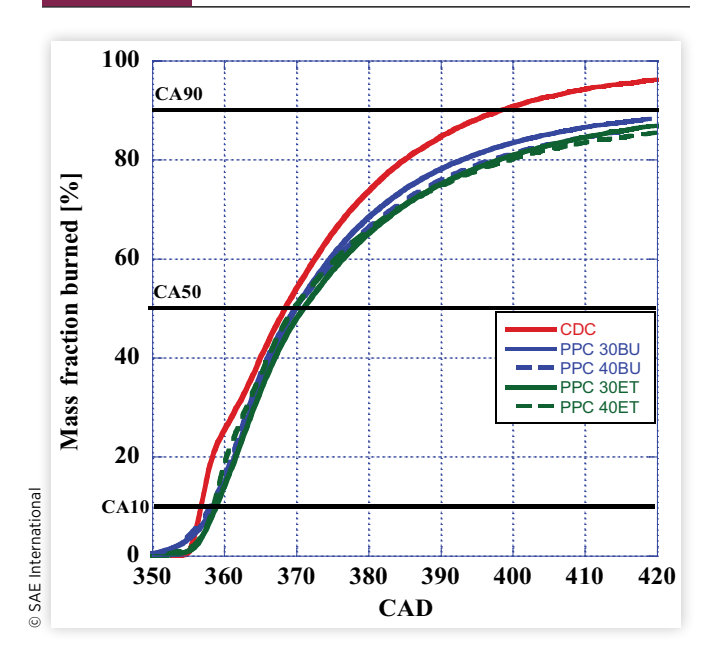
the 5 bar IMEP PPC experimentation, with the most predominant dual peak AHRR with PPC 40ET, and the n-butanol experiments are all extended with no defined peaks. These results are confirmed by Cheng et al. [61] with their results using n-butanol and diesel with a DI of 8°BTDC.

It was found that for both loads of 4 bar and 5 bar IMEP, PPC with ethanol had no heat release occur prior to the second DI event, unlike n-butanol which had both LTHR and HTHR occur prior to the second DI event. As PFI % was increased for n-butanol for both loads, LTHR had a shorter duration whereas ethanol only had this occur at a higher load of 5 bar IMEP with the inverse effect at 4 bar IMEP. This indicates that for greater control of PPC with n-butanol, a greater PFI % is needed to prevent HTHR from occurring prior to the second injection event (to prevent pre-ignition phenomena) compared to ethanol; however, ethanol had LTHR occur for a shorter duration than n-butanol leaving more fuel available for HTHR which could lead to an increase in NOx emissions from PPC with ethanol.

Mass Fraction Burned

Mass Fraction Burned (MFB) was determined by integrating the AHRR at the beginning of HTHR, as seen in Soloiu et al. [60] with UHC emissions determining the maximum MFB achieved per combustion event. CA50 was set at 9°ATDC as a combustion phasing constraint condition for this investigation with a tolerance of ±2 CAD, Figure 25 contains the MFB for all combustion experiments conducted at a load of 4 bar IMEP. It was observed that CA50 for all combustion experiments conducted at 4 bar IMEP was within the set of constraints for this investigation, with PPC 30 ET having the greatest deviation of +2 CAD from the set point of 9°ATDC





as shown in <u>Table A.4</u>. PPC 30ET had the greatest deviation of CA50 (11°ATDC) as a result of both the low PFI % used in conjunction with the lower DCN of ethanol compared to n-butanol. This led to a state where an SOI-2 earlier than 9°BTDC would have resulted in a greater deviation of CA50 below 9°ATDC in conjunction with an increase in PRR and RI as ethanol, despite having the lowest DCN of the low-reactivity fuels used for PPC, and had a greater PRR and RI compared to n-butanol per PFI % used. The ID shown in <u>Table A.5</u> was calculated from the start of SOI-2 to CA10 and CD was determined from CA10 to CA90.

As observed in <u>Table A.2</u>, PPC with either n-butanol or ethanol at a late target CA50 of 9°ATDC had a decreased ID. This is supported by the AHRR graphs where it was observed that PPC with n-butanol experienced a greater quantity of pre-ignition of the homogeneous air/fuel mixture as was prominently shown with PPC 40BU, where ID was 3 CAD indicating HTHR had begun prior to SOI-2. Ethanol, on the other hand, had less LTHR and HTHR occur prior to SOI-2 for 30% PFI; nevertheless, ethanol had a greater PRR and slope of AHRR similar to CDC.

This indicates that a late CA50 of 9°ATDC at a low load is unstable and is predominantly controlled by the interaction of the PFI fuel and pilot DI (SOI-1) autoigniting rather than SOI-2, leading to the combustion event with PFI of low-reactivity fuel increasing the ID as seen in other PPC studies [7]. As a result of the late CA50 of 9°ATDC and the low load, CA90 was not achieved by all PPC experiments conducted for both n-butanol and ethanol and led to an increase in UHC as observed in the emissions study further on. This can be observed in Figure 25 where MFB had a greater slope between CA10 and CA50 than ULSD CDC; however, as pressure and temperature decrease as the cycle progresses past TDC, the remaining n-butanol/ethanol in the combustion chamber that was not combusted from the initial flame front

either from quenching of the flame at the walls of the combustion chamber or air/fuel mixture trapped in the crevices remain unburnt.

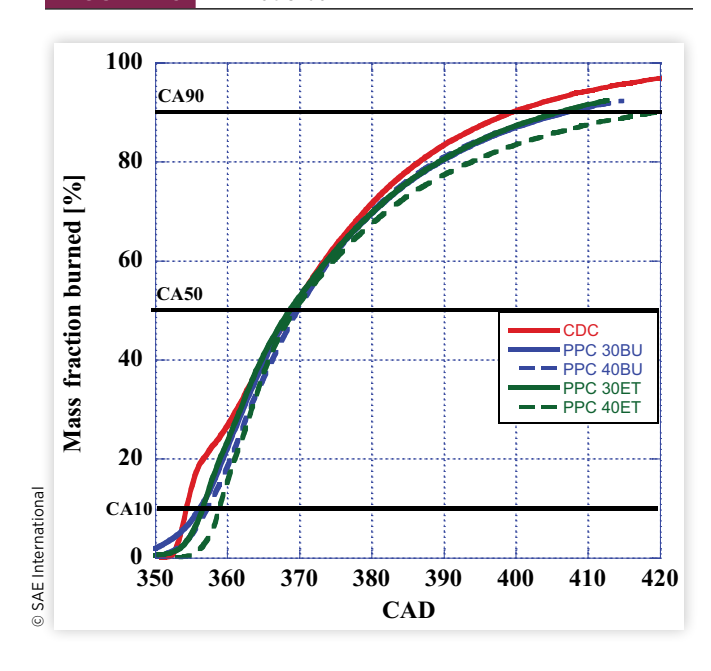
PPC at a higher load of 5 bar IMEP, however, had more desirable combustion characteristics as shown in <u>Figure 26</u> and <u>Table A.5</u>. All combustion methods investigated at 5 bar IMEP did achieve a CA50 of 9 CAD as set for the boundary condition of this investigation.

It was shown that the higher load used for these combustion experiments led to fewer deviations in MFB as shown in Figure 26 between CA20 and CA60. The ID however was lower for all PPC experiments than CDC due to the phenomena previously described contrary to typical PPC characteristics of increasing ID from the introduction of the low-reactivity fuel to the combustion chamber. This is due to both the lower quantity of PFI % used and the advanced CA50 of 9°ATDC, as a result, LTHR and HTHR occurred prior to SOI-2 for n-butanol as seen in the before mentioned AHRR graphs.

As for PPC with ethanol, minimal LTHR and HTHR occurred prior to SOI-2 but had an elevated PRR and AHRR slope more similar to CDC than PPC with n-butanol as observed with PPC 30ET.

All PPC experiments conducted at a load of 5 bar IMEP, achieved MFB past 90% contrary to what was observed at 4 bar where the maximum MFB achieved was 88.2% for PPC 30BU. Similar to ID, PPC had a prolonged CD compared to CDC. PPC 30BU was able to achieve a CD of 51 CAD with an increase in PFI to 40% leading to a decrease of 1 CAD to CD. This indicates that for a CA50 of 9°ATDC, the n-butanol CD is not heavily affected by the increase in PFI %; however, this increase in PFI % leads to pre-ignition and an invalid ID. PPC with ethanol on the other hand had an increase of CD from 50 CAD at a PFI % of 30% to 60 CAD at a PFI % of 40% whereas the ID only increased from 8 CAD to 9 CAD,

FIGURE 26 MFB at 5 bar IMEP.



indicating that ethanol is more heavily influenced by PFI % than n-butanol for CD; this could be a disadvantage as the increase in CD leads to greater heat losses to the engine components as well as lower MFB leading to higher UHC emissions.

In-Cylinder Temperatures

The in-cylinder temperature results obtained for all combustion experiments conducted at both 4 bar and 5 bar IMEP were derived from the in-cylinder pressure data obtained. The in-cylinder temperatures for both PPC and CDC at a load of 4 bar IMEP were graphed in Figure 27. It can be seen that, as a general trend, the introduction of the low-reactivity fuel via PFI reduces the intake air/fuel charge into the combustion chamber compared to CDC. n-Butanol reduced in-cylinder temperatures with a PFI of 40% while ethanol achieved a similar cooling effect at both 30% and 40% PFI due to its higher latent heat of vaporization. However, since a late CA50 was chosen for this investigation, only ethanol was shown to decrease peak combustion temperatures compared to CDC at a load of 4 bar IMEP due to its lower reactivity. PPC with n-butanol, on the other hand, had an increase of in-cylinder temperatures with a maximum increase in temperature to CDC of 45°C for PPC 40BU. The increase in in-cylinder temperatures for n-butanol occurred from both a combination of having a peak pressure similar if not exceeding that of CDC but also the pre-ignition of n-butanol that was observed in both the AHRR and MFB.

For a higher load of 5 bar IMEP, as shown in Figure 28, the cooling effect of the intake air/fuel charge has a greater effect than at a lower load due to the increase in PFI mass injected. As a result, all PPC methods tested achieved lower initial in-cylinder temperatures than CDC with a greater delta

FIGURE 27 In-cylinder temperatures at 4 bar IMEP.

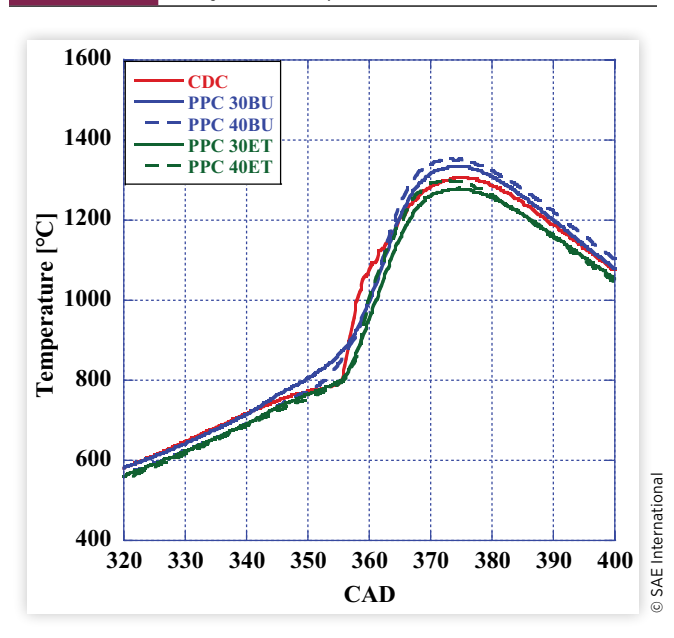
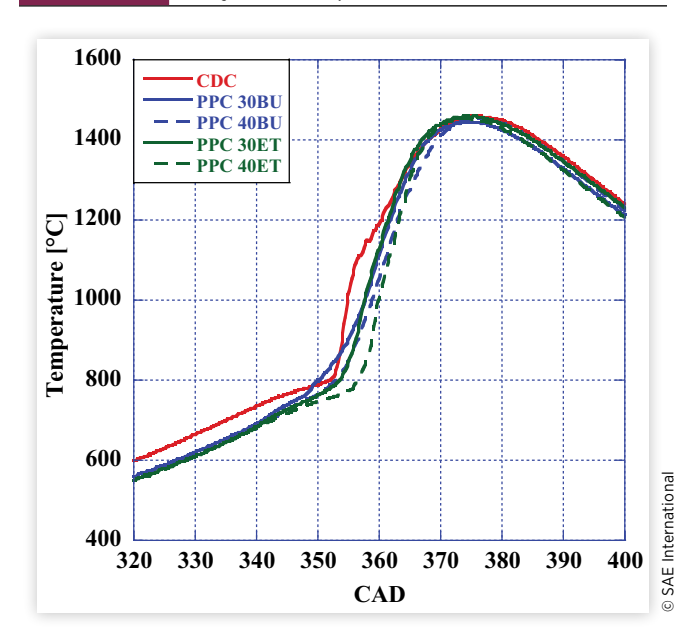


FIGURE 28 In-cylinder temperatures at 5 bar IMEP.



temperature of 35°C. It was shown that PPC 30ET had the same peak temperature as CDC at 1460°C whereas the lowest peak temperature was PPC 30BU at 1445°C. As PFI % increased to 40%, ethanol decreased its peak temperature to 1455°C and n-butanol had an increase in peak temperature to 1453°C. This indicates that, for a higher load, ethanol can decrease peak in-cylinder temperatures as PFI % increases and n-butanol has the inverse reaction to PFI % increases at higher loads. This reduction in in-cylinder temperatures is also due to the retarded combustion phasing caused by the PFI of alcohols. As indicated in the AHRR in Figure 23, CDC has the narrowest area under the curve, reaching HTHR in a shorter period compared to the PPC experiments where their combustion is occurring over a wider CAD increment. These in-cylinder cooling effects are occurring due to the significant delays in combustion phasing confirmed by Zhang et al. [62].

Heat Losses

As is common with LTC methods, thermal efficiencies and the associated heat losses are often a point of concern [63, 64]. Due to this, an investigation on heat transfer losses was conducted on the three combustion experiments with the highest MFB observed. The heat transfer losses were calculated utilizing Equations 6 and 7 based on investigations conducted by Borman and Nishiwaki on the modeling of convection- and radiation-based losses with additional improvements made by Soloiu et al. $[\underline{46}, \underline{48}]$. The models were utilized to identify the heat transfers associated with the convection of gases to the combustion chamber walls and the radiation emitted from diffusion flames and PM. The overall heat flux (\dot{q}) was determined using Equation 6 where the wall temperature (T_W) was assumed to be an average temperature and the combustion temperatures (T_A) and the air thermal conductivity (λ_A) were determined from experimental data. Viscosity was obtained by a Sutherland model where the results of which were utilized for calculating heat fluxes. The Reynolds number needed for the calculation of overall heat flux was calculated utilizing Equation 7 [60].

$$\dot{q}(\alpha) = A \frac{\lambda_A(\alpha)}{D} Re^{0.7} \left(T_A(\alpha) - T_W \right) + \sigma * \varepsilon \left(T_A^4(\alpha) - T_W^4 \right)$$
Eq. (6)

$$Re(\alpha) = \rho(\alpha) \frac{S * N * D}{30\mu(\alpha)}$$
 Eq. (7)

As seen in Figure 29, only PPC 30ET had a slightly higher total heat flux than CDC despite having similar combustion temperatures. The increased total flux of PPC 30ET (1.77% over CDC) therefore is a result of the increased total DI time of PPC 30ET (1.04 ms) compared to CDC (0.87 ms) as it can also be seen that PPC 40BU had a decreased total flux of 2.29% compared to CDC due to both the lower combustion temperatures and lower total DI time (0.75 ms).

The reduction of DI duration for PPC 40BU resulted in lower turbulence introduced from the DI of fuel into the combustion chamber. The convection fluxes observed in Figure 29 showed that PPC 30ET had an increase in convection flux of 2.05% compared to CDC and an increase of 2.43% over PPC 40BU.

The increase in convection fluxes for PPC 30ET is due to both the longer injection time over PPC 40BU and the second injection event occurring earlier in the cycle, thus having more engine wall surface area exposed for convection losses to occur, as also experienced by Singh et al. [65].

As for the radiation fluxes, it was observed that although the peak fluxes from all three combustion

experiments were indiscernible to one another, CDC had higher radiation fluxes at 355 CAD than PPC 30ET and PPC 40BU due to the higher peak AHRR observed from the high temperature diffusion flame. PPC 30ET, on the other hand, had the second highest radiation fluxes at 363 CAD due to a mixture of diffusion and premixed flames occurring, leading to an overall reduction of flame temperature; however, compared to PPC 40BU, PPC 30ET had a higher temperature flame due to increased reliance on diffusion flames for combustion.

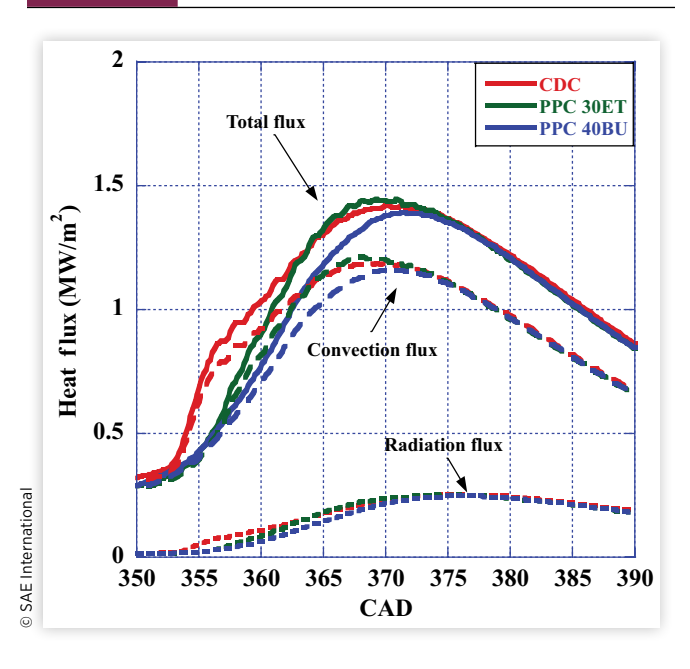
Peak radiation fluxes for PPC 30ET and PPC 40BU were able to increase to the same magnitude as CDC due to the greater magnitude of heat release occurring ATDC leading to more radiation losses as more surface area of the engine walls is exposed [66].

It was observed in Figures 30, 31, and 32 and Table 14 that CDC at a load of 5 bar IMEP had the highest heat loss of the three experiments observed with a notable higher loss for convection compared to both PPC 30ET and PPC 40BU. PPC 30ET and PPC 40BU had similar radiation, convection, and crevice losses at 4%, 16.3% (±1%), and 1.4%, respectively, while CDC had losses at 4.7%, 19.3%, and 1.5%, respectively.

Although PPC 30ET and PPC 40BU had both different PFI % and low-reactivity fuels, their respective heat losses were nearly identical because of the fundamental combustion characteristics of PPC.

The difference in heat losses for CDC with respect to PPC is indicative of the dissimilar fundamental combustion properties of each method as a result PPC had lower radiation and convection heat losses due to lower reliance on diffusion combustion. This is primarily done so for the reduction of soot emissions as was indicated by the lower radiation losses observed.

FIGURE 29 Heat fluxes at 5 bar IMEP.



Emissions

Emissions were measured at engine out with no aftertreatment system utilized to observe the effects of the various combustion experiments conducted at loads of 4 bar and 5 bar IMEP. An MKS 2030 was used to measure gaseous emissions such as NOx, CO, UHC, $\rm CO_2$, and formaldehyde while an AVL Model 483 Micro Soot Sensor apparatus was utilized to measure soot emissions from the engine at the defined steady-state condition outlined in the Experimental Setup.

Soot Emissions

The soot emissions were measured for all combustion experiments conducted at a load of 4 bar and 5 bar IMEP utilizing an AVL 483 Micro Soot Sensor, the results of which can be seen in Figures 33 and 34.

It can be observed at a load of 4 bar and 5 bar IMEP that all PPC methods tested achieved lower soot emissions than CDC with a minimum reduction of 69.75% (-1.123 g/kWh) at 4 bar and 37.72% (-0.659 g/kWh) at 5 bar.

FIGURES 30, 31, 32 Heat losses from combusted fuel at 5 bar IMEP.

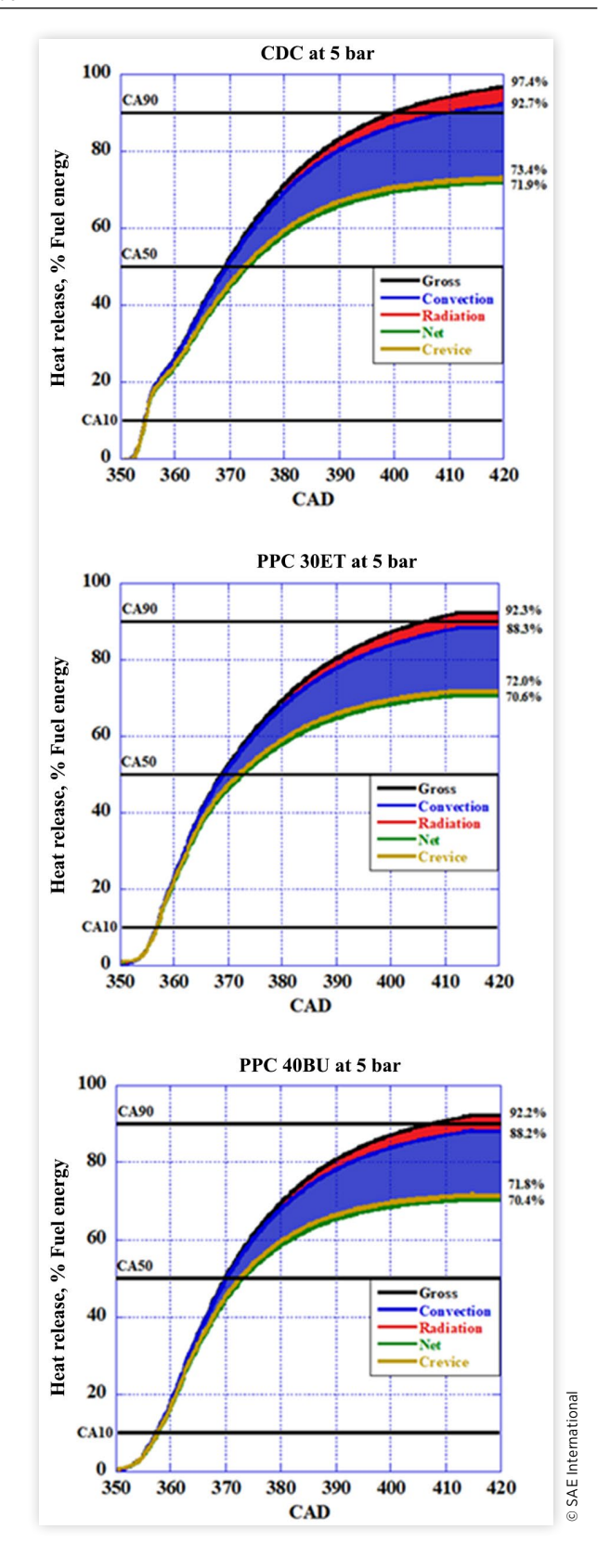


TABLE 14 Heat loss percentages from combusted fuel at 5 bar IMEP.

Losses	CDC [%]	PPC 30ET [%]	PPC 40BU [%]
Radiation	4.7	4.0	4.0
Convection	19.3	16.3	16.4
Crevice	1.5	1.4	1.4

© SAE International

FIGURE 33 Soot emissions at 4 bar.

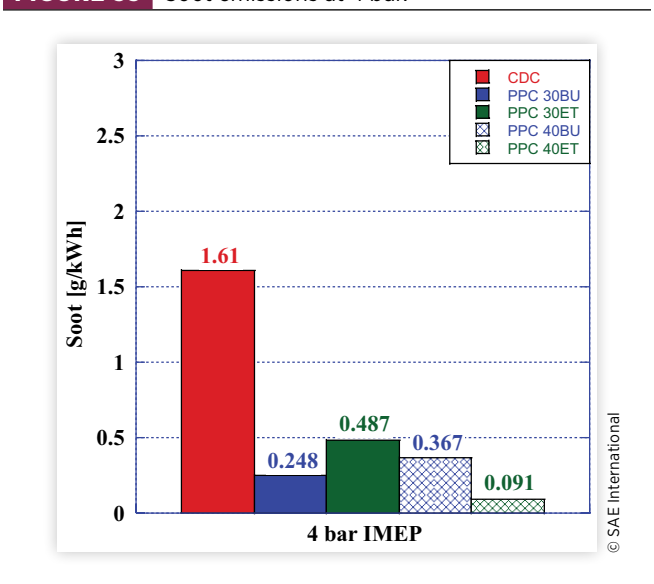
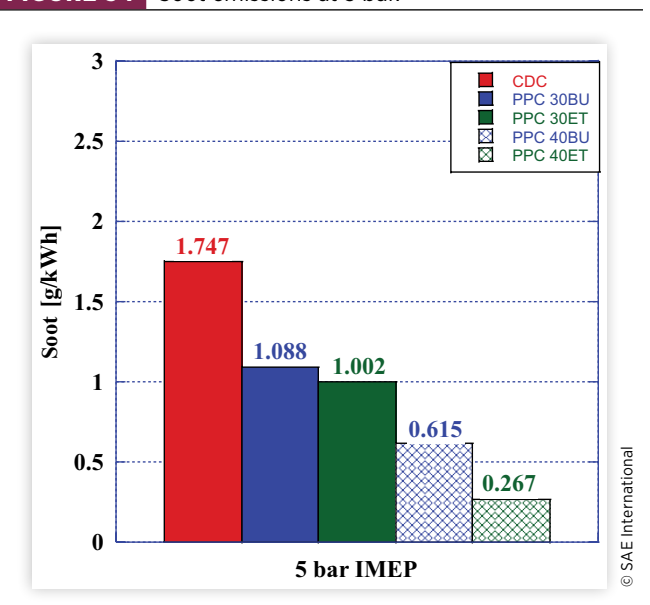


FIGURE 34 Soot emissions at 5 bar.



PPC 40ET had the greatest reduction of soot emissions from CDC for both loads with a reduction of 94.34% (–1.159 g/kWh) at 4 bar IMEP and 84.71% (–1.480 g/kWh) at 5 bar IMEP. It was shown both in Figures 33 and 34 and Table A.6 that PPC with ethanol had a reduction of soot emissions as PFI % was increased for both loads at 4 bar and 5 bar while PPC with n-butanol had the inverse relation at 4 bar IMEP and the same relation at 5 bar IMEP. This indicates that the higher oxygen content of ethanol is beneficial for lowering soot emissions as PFI % is increased and is particularly more effective at higher loads.

The observations made during this section indicate that although PPC with either n-butanol or ethanol can simultaneously reduce NOx and soot emissions, ethanol was shown to have greater reductions of soot emissions due to its higher oxygen content. However, PPC with n-butanol may be able to achieve similar soot emissions reductions with additional amounts of PFI % or boost added. N-butanol has resulted in greater combustion stability as shown by the AHRR and PRR results.

NOx Emissions

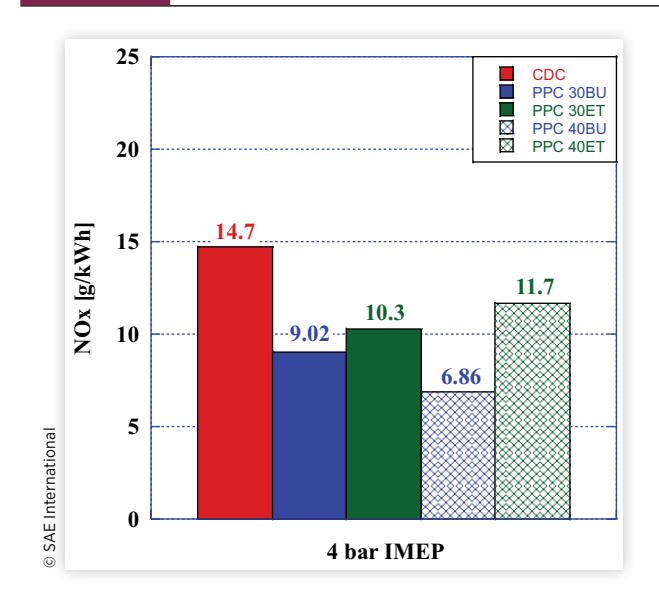
NOx emissions were measured for CDC, PPC 30BU, PPC 30ET, PPC 40BU, and PPC 40ET at a load of 4 bar and 5 bar IMEP as seen in Figures 35 and 36. It can be seen in Figures 35 and 36 for a load of 4 bar IMEP that all PPC experiments conducted were able to reduce NOx emissions compared to CDC between a range of 20.40% and 53.33% as observed in Table A.7. For both PFI % used for PPC experiments conducted at 4 bar and 5 bar IMEP, PPC with n-butanol had lower NOx emissions compared to PPC with ethanol, with the greatest reduction in NOx emissions occurring with PFI at 40% as seen in Table A.7.

The lower NOx emissions observed for PPC with n-butanol at 4 bar IMEP occurred despite PPC 30BU and PPC 40BU having greater peak combustion temperatures than PPC 30ET, PPC 40ET, and CDC. This could possibly be explained by the lower peak AHRR observed in Figure 17 where PPC with n-butanol had a lower peak AHRR than PPC with ethanol at each respective PFI % due to the extended LTHR events.

The extended AHRR events are caused by the cooling effects the PFI alcohols induce on the combustion chamber before they are ignited with the DI of ULSD. These cooling effects reduce NOx emissions produced in-cylinder. At a load of 5 bar IMEP, NOx emissions were reduced even further for PPC with n-butanol by as much as 62%. While NOx emissions were decreased for PPC with ethanol compared to CDC, NOx emissions increased as the load increased contrary to the trend observed for PPC with n-butanol. This occurred not only because of PPC with n-butanol has lower in-cylinder temperatures than PPC with ethanol at their respective PFI % but rather due to the lower intensity of HTHR that occurred.

This extension of the AHRR is also caused by the CAD range for which the second DI occurs. If the injection occurs

FIGURE 35 NOx emissions at 4 bar.

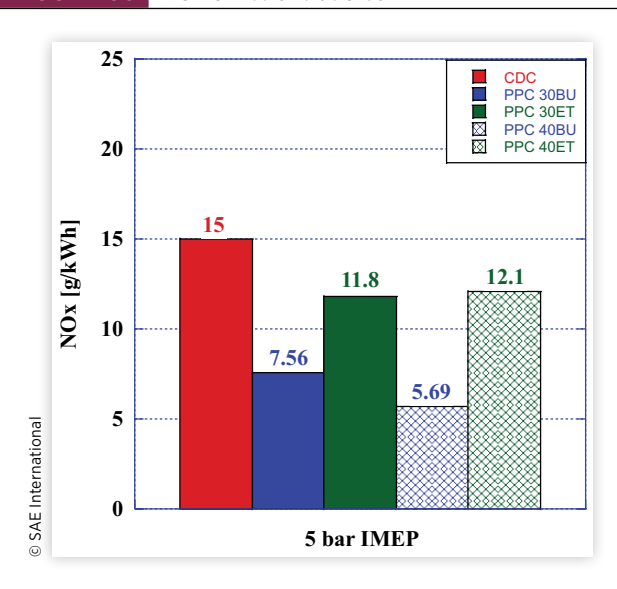


in the range of 12°BTDC to 6°BTDC, the AHRR has less of a peak and the combustion flame front combusts over a longer CAD range. These extended combustion phases are linked to better NOx emissions [61, 62].

It was further observed that PPC with ethanol was not as affected by PFI % as n-butanol. Contrary to this trend, PPC with ethanol had a rise in NOx emissions occur of 0.3 g/kWh from PPC 30ET to PPC 40ET due to the elimination of LTHR and subsequent increase of HTHR. The increase in NOx emissions for PPC with ethanol could also be attributed to the increased PPRR previously observed.

Although PPC with ethanol had shown improvements in soot emissions, it did result in more NOx emissions than PPC with n-butanol, yet the results are still lower than CDC. It was

FIGURE 36 NOx emissions at 5 bar.

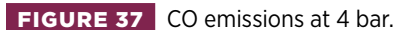


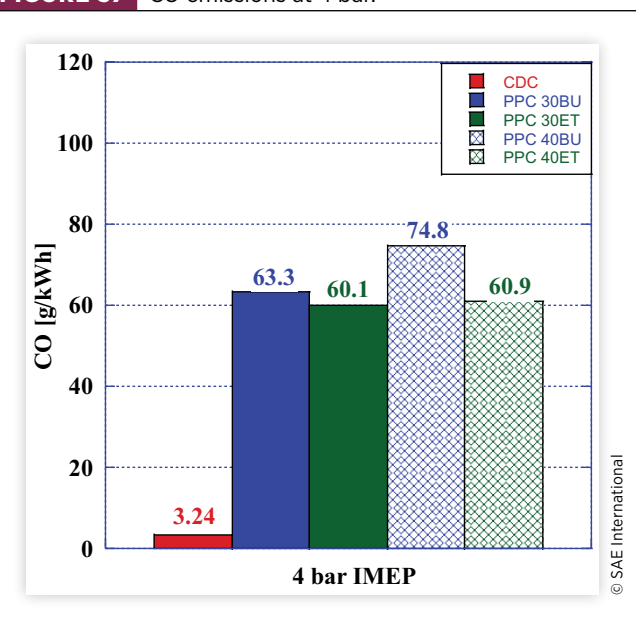
also observed that as PFI % was increased, PPC with ethanol had NOx emissions increase. PPC with n-butanol had NOx emissions decreased with PFI % increase from 30% to 40%. At a load of 4 bar IMEP, PPC 30ET and PPC 40BU had the lowest NOx emissions for their respective fuels at 10.3 g/kWh and 6.9 g/kWh, respectively. At a load of 5 bar IMEP, the trend remained the same with PPC 30ET having the lowest NOx emissions for PPC with ethanol and PPC 40 BU for PPC with n-butanol with NOx emissions at 11.8 g/kW h and 5.7 g/kWh, respectively.

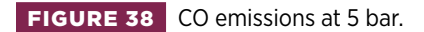
CO Emissions

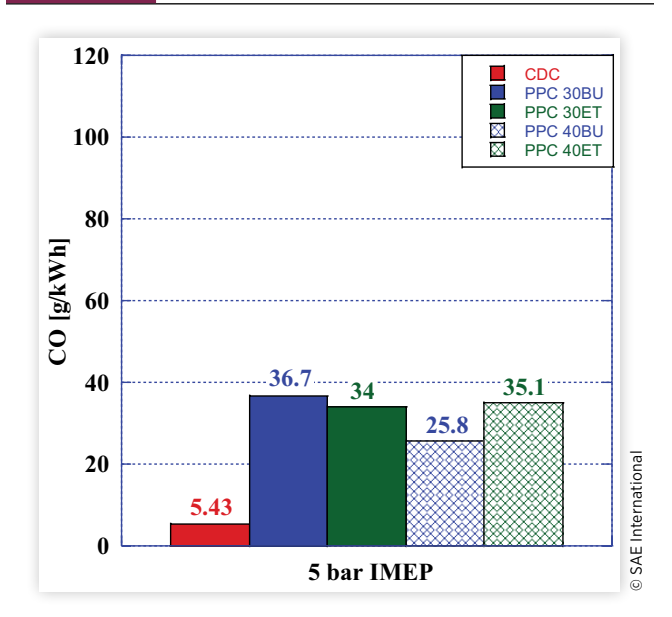
CO emissions were measured for all combustion experiments conducted at 4 bar and 5 bar IMEP and are shown in Figures 37 and 38. PPC was observed to have higher CO emissions than CDC at both 4 bar and 5 bar IMEP, CO emissions were elevated for PPC due to lower MFB resulting from a late CA50 of 9°ATDC used for this investigation. It was observed that PPC with n-butanol at 4 bar IMEP had higher CO emissions than ethanol at both PFI % of 30% and 40% and that CO emissions increased as PFI % increased. Ethanol, however, not only had lower CO emissions than n-butanol but also had a slight increase in CO emissions as PFI % increased.

At a load of 5 bar IMEP, it can be seen in Figures 37 and 38 that the increase in CO emissions for all PPC experiments conducted had a smaller increase over CDC CO emissions compared to the emissions observed at a load of 4 bar IMEP. This observation can be explained by the higher MFB previously observed for a load of 5 bar IMEP, thus indicating that as the load increases less incomplete combustion processes occur throughout the combustion chamber. Furthermore, it was observed that PPC with n-butanol had a decrease in CO emissions as PFI % was increased while ethanol had a slight increase in CO emissions as PFI % was increased. This reflects







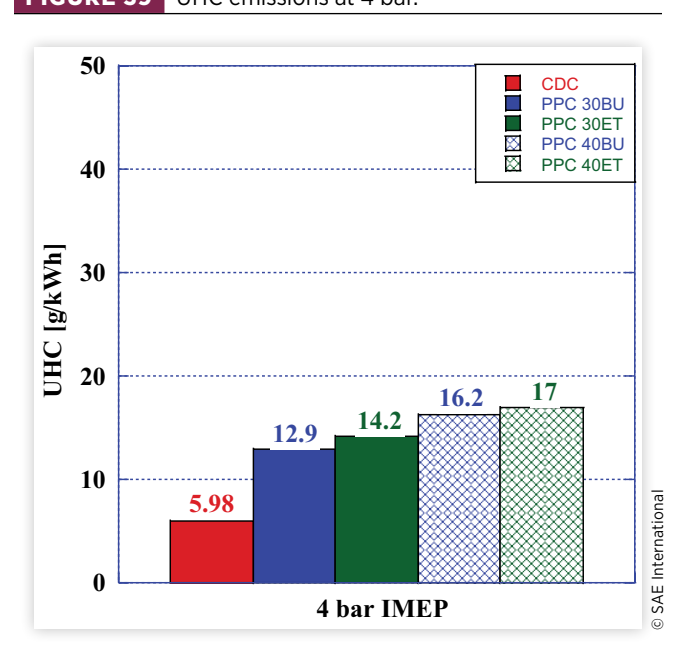


the previous observation with MFB where an increase in PFI % for ethanol resulted in a lower MFB and thus more incomplete combustion products.

UHC Emissions

UHC emissions from PPC are a common point of contention, and thus any possible reduction to these emissions with the utilization of different PFI fuels or PFI % is desired to allow for the reduction of other emissions. As is the case, UHC emissions were measured for a load of 4 bar and 5 bar IMEP with ethanol and n-butanol at PFI % of 30% and 40% compared to CDC, as seen in Figure 39. It was observed that for a load

FIGURE 39 UHC emissions at 4 bar.

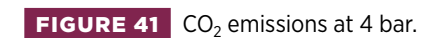


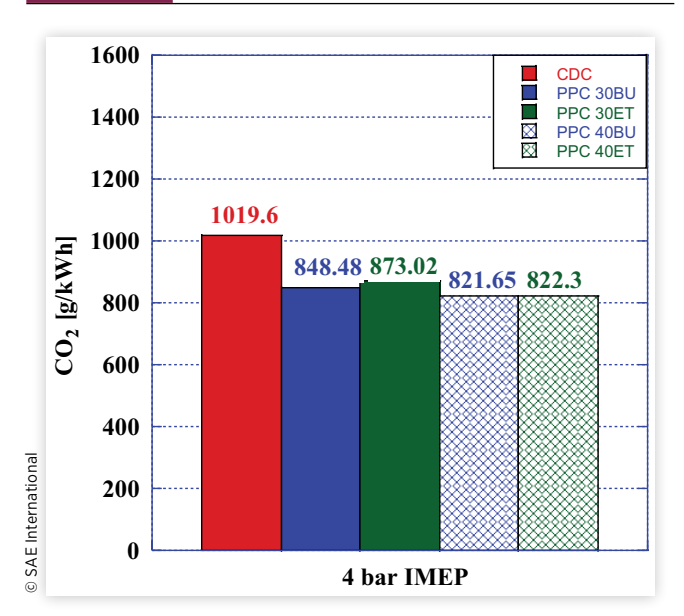
of 4 bar IMEP, PPC with ethanol had greater UHC emissions than n-butanol by 1.3 g/kWh and 0.8 g/kWh at PFI % of 30% and 40%, respectively. This indicates that for a lower load of 4 bar IMEP, n-butanol is preferable for UHC emissions control of PPC and should be done at lower PFI % to reduce UHC as an increase in UHC emissions leads to lower MFB and combustion efficiency.

Although UHC emissions were elevated for PPC at 5 bar IMEP compared to CDC, there was a reduction in UHC emissions when compared to a lower load of 4 bar IMEP, as can be seen in Figures 39 and 40. The increase in load to 5 bar IMEP results in PPC with ethanol having lower UHC emissions compared to PPC with n-butanol at a PFI of 30% by a reduction of 0.51 g/kWh. However, this reduction only appears for a PFI of 30% whereas, at a PFI of 40%, PPC 40BU had lower UHC emissions than PPC 40ET by 0.5 g/kWh. This could be a result of the lower reactivity of ethanol than that of n-butanol, resulting in less complete combustion of the air/fuel mixture as higher PFI % is used at a load of 5 bar IMEP.

CO₂ Emissions

 $\mathrm{CO_2}$ emission mitigation methods have become an important factor in combating climate change as regulations by government entities become ever more stringent on the quantity of $\mathrm{CO_2}$ emissions emitted by ICEs. As such, alternative combustion methods and carbon-neutral fuel sources have been investigated for their potential on reducing this harmful greenhouse. In <u>Figures 41</u> and <u>42</u>, the $\mathrm{CO_2}$ emissions from the combustion experiments conducted at a load of 4 bar and 5 bar IMEP can be seen, where it was observed that all PPC experiments conducted had a reduction in $\mathrm{CO_2}$ emissions compared to CDC. PPC 40ET and PPC 40BU had the lowest





 CO_2 emissions of all the experiments conducted at a load of 4 bar IMEP with a reduction of 19.4% compared to CDC. n-Butanol versus ethanol at a PFI % of 40% had shown minimal differences in CO_2 emissions falling within 0.65 g/kWh of each other while, at a PFI of 30%, ethanol had greater CO_2 emissions than n-butanol by 24.54 g/kWh.

At a load of 5 bar IMEP, all four PPC experiments conducted were within 45.37 g/kWh of each other with PPC 40ET having the lowest $\rm CO_2$ emissions at 819.17 g/kWh (13.9% lower than CDC) and PPC 30ET at the higher end at 864.54 g/kWh (9.1% lower than CDC). PPC with n-butanol had a

FIGURE 40 UHC emissions at 5 bar.

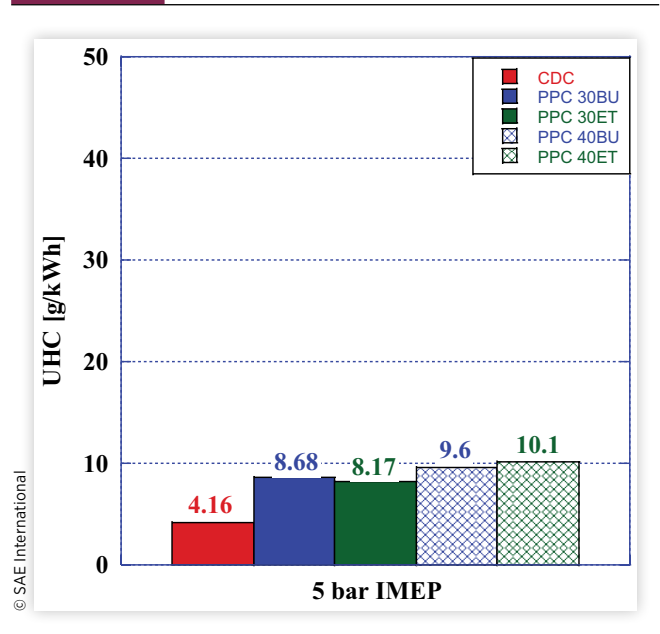
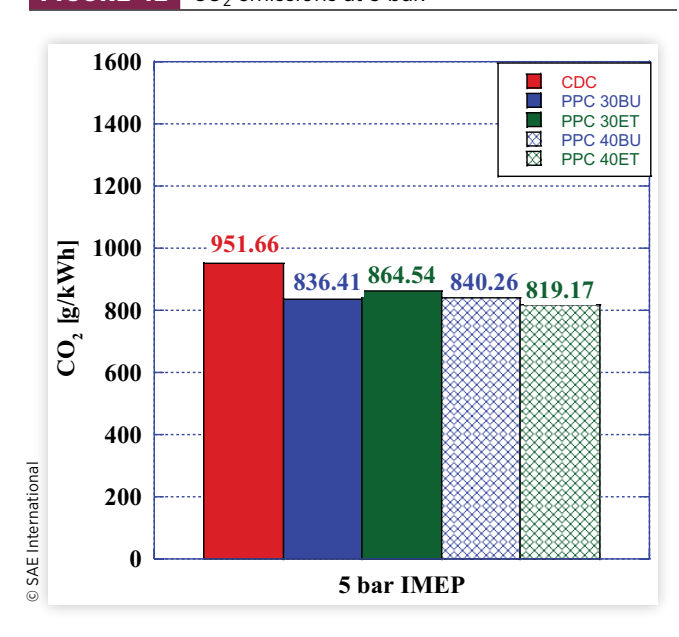


FIGURE 42 CO₂ emissions at 5 bar.



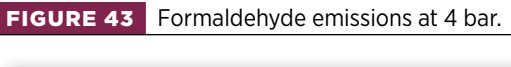
minor increase of 3.85 g/kWh in CO_2 emissions from a PFI of 30% to 40%, whereas PPC with ethanol had a reduction of 45.37 g/kWh as PFI % increased.

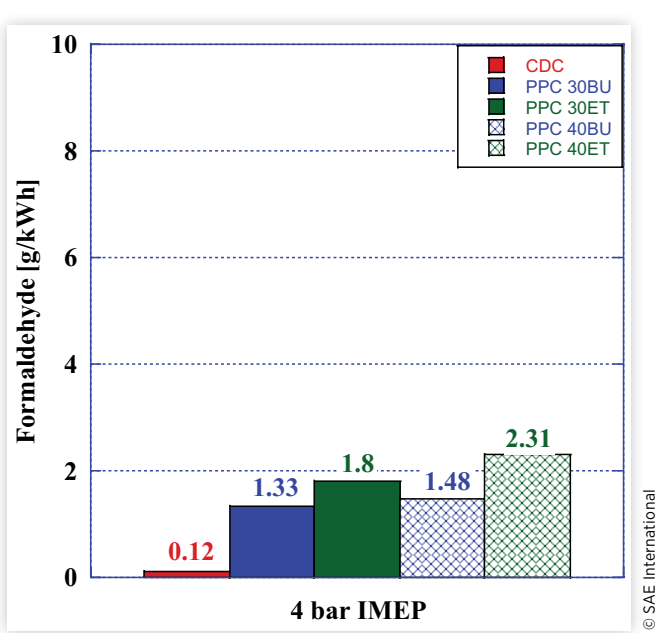
The CO₂ emissions from PPC, however, cannot be equivalently compared to CDC at face value as a portion of the carbon available to the system from the fuels injected comes from carbon-neutral renewable sources such as the first- and second-generation bio-alcohols ethanol and n-butanol, respectively. The total number of moles of carbon available from all injected fuels per combustion experiments was assembled in Table A.8 where the percentage of carbon attributed from ULSD and renewable PFI bio-alcohols can be observed. As observed from Table A.8, it can be seen that the total number of moles of carbon available for combustion is higher for all PPC experiments conducted at 4 bar IMEP; however, the quantity of carbon from nonrenewable ULSD is reduced compared to CDC for all PPC experiments conducted. PPC at a PFI of 30% had a reduction of nonrenewable carbon of 17.8% for PPC 30BU and 17.3% for PPC 30ET. The reduction of carbon derived from nonrenewable sources is further reduced as PFI is increased to 40%, where it is observed that PPC 40BU had a reduction of 29.9% and PPC 40ET had a reduction of 29.7%. In addition, it was observed that at 5 bar IMEP, PPC conducted with PFI at 40% with either n-butanol or ethanol had fewer moles of carbon available for combustion than CDC and, as a direct result, led to further reductions in nonrenewable carbon of 38.8% for PPC 40BU and 33.2% for PPC 40ET.

The findings of this investigation indicate that PPC reduces CO₂ emissions regardless of the load and PFI % utilized. Additionally, it was found that the environmental impact of PPC is lessened compared to CDC (nonrenewable carbon from ULSD) due to lower nonrenewable carbon fuel sources. At higher loads and PFI %, it was observed that ethanol and n-butanol had reduced the total number of moles of carbon while lowering CO₂ emissions, NOx, and soot emissions simultaneously. This combination makes PPC with bio-alcohols a more sustainable solution for meeting future emissions regulations and reducing climate change with the use of second-generation bio-alcohols (n-butanol).

Formaldehyde Emissions

Formaldehyde emissions, although unregulated for auto emissions, are an important consideration for alternative combustion methods that utilize bio-alcohols. It was observed in Figures 43 and 44 that PPC formaldehyde emissions were higher than CDC at a load of 4 bar and 5 bar IMEP. PPC with n-butanol had lower formaldehyde emissions than PPC with ethanol at both 30% and 40% PFI, PPC 30BU had the lowest formaldehyde emissions of the PPC experiments conducted at 1.33 g/kWh at 4 bar IMEP. PPC 40BU had the lowest formaldehyde emissions of the PPC experiments at a load of 5 bar IMEP at 0.78 g/kWh. PPC with ethanol, on the other hand, had elevated formaldehyde emissions compared to n-butanol at each





PFI % with PPC 30ET having an increase in formaldehyde emissions of 0.47 g/kWh over PPC 30BU at 4 bar IMEP. As PFI was increased to 40%, formaldehyde emissions for PPC 40BU and PPC 40ET increased by 0.15 g/kWh and 0.51 g/kWh, respectively, at 4 bar IMEP while, at 5 bar IMEP, only ethanol had increased emissions by 0.34 g/kWh. The decrease in formaldehyde emissions at higher loads of 5 bar IMEP is a result of the lower UHC and increase in the combustion efficiency of PPC at a higher load.

FIGURE 44 Formaldehyde emissions at 5 bar.

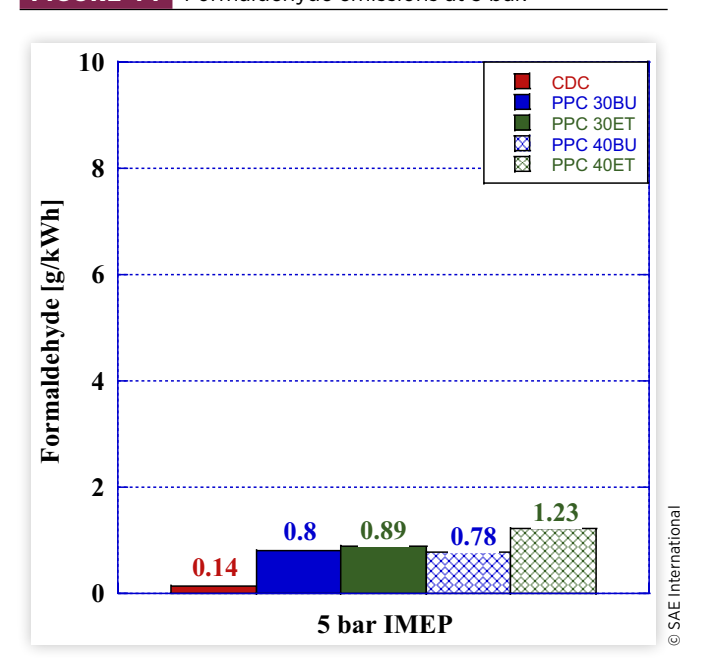


FIGURE 45 ESFC of the five combustion experiments conducted at 4 bar IMEP.

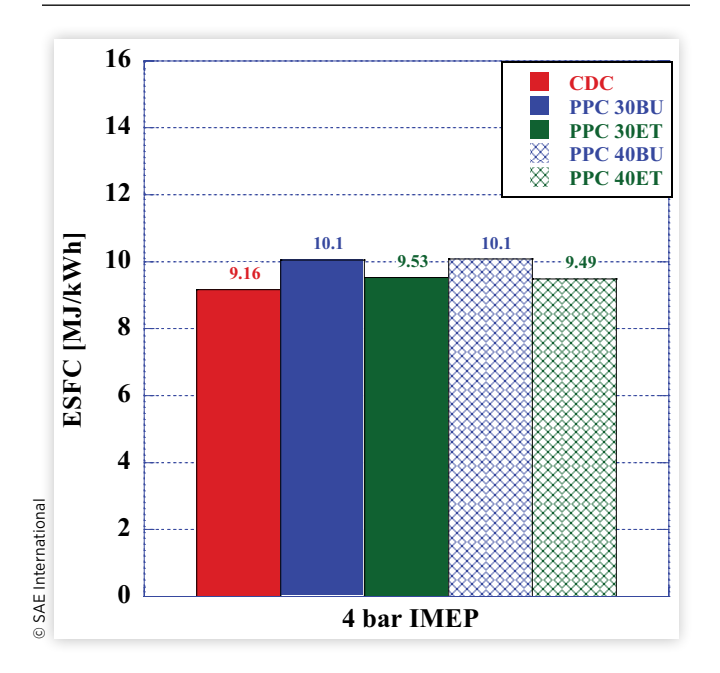
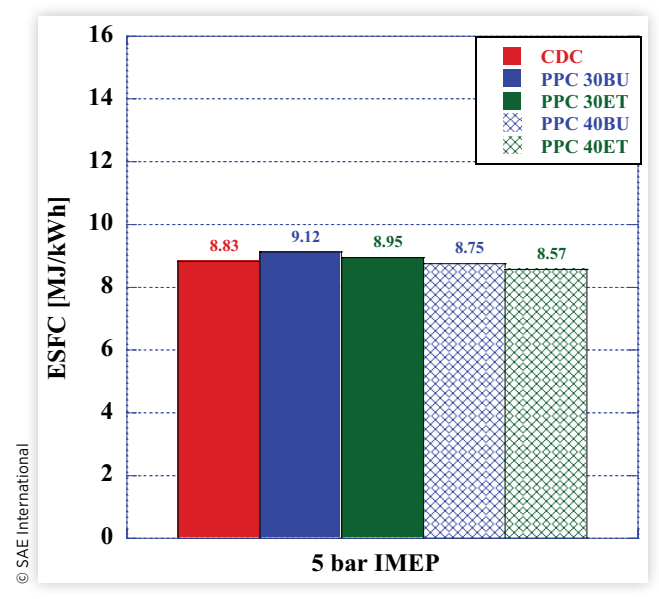


FIGURE 46 ESFC of the five combustion experiments conducted at 5 bar IMEP.



Fuel Consumption and Efficiency

Energy Specific Fuel Consumption

The Energy Specific Fuel Consumption (ESFC) for each combustion test was calculated using the LHV of each fuel used, and the mass flow rate for both the DI and PFI fuel. The results of which are shown in Figure 45 for experiments conducted at 4 bar IMEP and Figure 46 for experiments conducted at 5 bar IMEP. It was seen in Figure 45 that all PPC experiments conducted had a higher ESFC than CDC by a range from 3.48% to 9.31% due to the lower energy content of either n-butanol or ethanol and the higher UHC emissions of PPC at a load of 4 bar IMEP. Although ESFC was higher for the four PPC experiments conducted at 4 bar IMEP, PPC with ethanol had lower ESFC than PPC with n-butanol due to its energy density. The decrease in ESFC for PPC with ethanol can also be explained by the greater peak AHRR observed when compared to PPC with n-butanol.

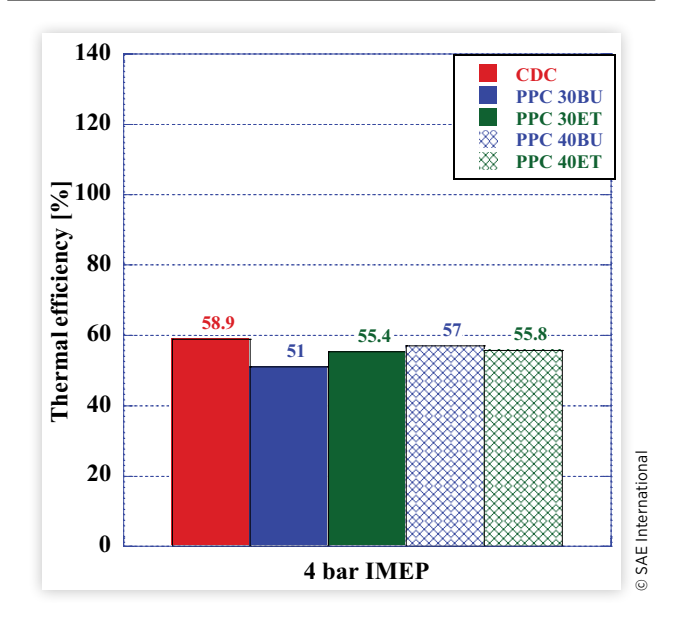
In <u>Figure 46</u> the ESFC for experiments was conducted at 5 bar IMEP where it can be seen that both PPC 40BU and PPC 40ET had lower ESFC than CDC by as much as 2.99%. The lower ESFC of PPC at 40% PFI for both n-butanol and ethanol is attributed to a higher percentage of less energy-dense fuel being utilized with minimal increases in fuel consumption.

Indicated Thermal Efficiency

The thermal efficiency for LTC methods is typically a point of contention as CDC typically has higher thermal efficiencies due to its lower CD and late SOI; however, with the proper PFI % and injection timing, PPC can achieve higher thermal efficiencies. At lower loads PPC was observed to have a slightly lower thermal efficiency compared to CDC, PPC with n-butanol had the lowest thermal efficiency at 51% with a 30% PFI at a load of 4 bar IMEP as observed in Figure 47. PPC with ethanol had a thermal efficiency greater than n-butanol at a PFI of 30% with a 4.4% increase in thermal efficiency; however, it was still lower than CDC by 3.5%. With an increase in PFI to 40% by mass, it was observed that thermal efficiency was raised for both PPC 40ET and PPC 40BU; however, PPC 40BU had the greatest increase in thermal efficiency by 6%. Ethanol, on the other hand, only had an increase in thermal efficiency of 0.4%, this resulted in n-butanol having the greatest thermal efficiency of all PPC experiments conducted at 4 bar IMEP. PPC 40BU had the highest thermal efficiency of all PPC experiments conducted at 4 bar IMEP despite the lower maximum MFB. This can be attributed to PPC 40BU lower ID and late SOI-2 resulting in greater HTHR at or past TDC and reducing the loss of heat to the engine components.

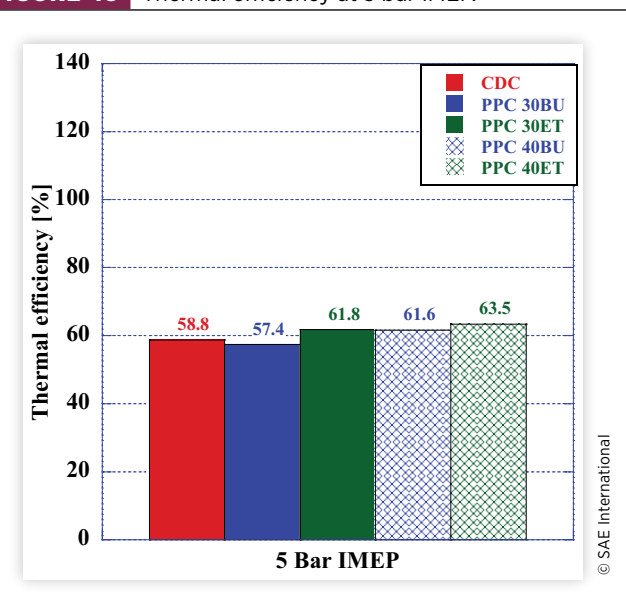
Thermal efficiency was increased for all PPC experiments conducted at a higher load of 5 bar IMEP as CDC had minimal changes to thermal efficiency as observed in <u>Figure 48</u>. It was observed that all PPC experiments, except for PPC 30BU, had a thermal efficiency greater than CDC, and as PFI % was increased, thermal efficiency was increased. Ethanol at both 30% and 40% had greater thermal efficiencies than CDC PPC

FIGURE 47 Thermal efficiency at 4 bar IMEP.



30BU and PPC 40BU, despite having greater ID and earlier SOI-2 for PPC. This can be attributed to both the lower reactivity of ethanol inhibiting the auto-ignition of the homogeneous air/fuel mixture prior to the main injection event as seen in the AHRR and the lower losses associated with convection and radiation compared to CDC. As PPC with ethanol has a greater ID than PPC with n-butanol, the heat loss of HTHR is decreased.

FIGURE 48 Thermal efficiency at 5 bar IMEP.



Conclusions

A comprehensive study was conducted on the combustion/ emissions characteristics of PPC with either n-butanol or ethanol at either 30% or 40% PFI by mass and CDC.

It was found in the combustion analysis investigation that PPC with either n-butanol or ethanol had several advantageous characteristics compared to CDC, such as PRR, RI, and AHRR. As the load was increased, LTHR and NTC regions were extended for PPC with n-butanol when comparing PPC with ethanol.

The PPRR values at a load of 4 bar and 5 bar IMEP for n-butanol at a 30% PFI are 2.3 bar/CAD and 3.4 bar/CAD. respectively, and the values with 40% PFI are 2.9 bar/CAD and 2.8 bar/CAD, respectively. The PPRR values at a load of 4 bar and 5 bar IMEP for ethanol at a 30% PFI are 2.6 bar/CAD and 5.0 bar/CAD, respectively, and the values with 40% PFI are 4.7 bar/CAD and 5.5 bar/CAD, respectively. The RI values at a load of 4 bar and 5 bar IMEP for n-butanol at a 30% PFI are 0.15 MW/m² and 0.39 MW/m², respectively, where the RI values at 40% PFI of n-butanol are 0.39 MW/m² and 0.15 MW/m², respectively. The RI values at a load of 4 bar and 5 bar IMEP for ethanol at a 30% PFI are 0.35 MW/m² and 0.69 MW/m², respectively, where the RI values at 40% PFI of n-butanol are 0.75 MW/m² and 0.64 MW/m², respectively. In PPC mode, PPRR and RI remained lower than in CDC mode. At 4 bar and 5 bar IMEP CDC has values of 1.48 MW/m² and 1.32 MW/m² for RI, respectively. Finally, the CDC values for PPRR for CDC in 4 bar and 5 bar are 5.79 bar/CAD and 6.76 bar/CAD, respectively.

PPC reduced NOx and soot emissions significantly compared to CDC. 40BU resulted in the greatest NOx emissions reductions with reductions 62.1% (–9.3 g/kWh) at 5 bar IMEP compared to CDC. The 40ET achieved the lowest soot emissions with reductions of 84.7% (–1.48 g/kWh) at 5 bar IMEP compared to CDC, respectively.

As is typical with LTC methods such as PPC, the reduction of NOx and soot emissions come at the cost of UHC emissions and CO emissions. In this study, it was observed that PPC had higher emission outputs of UHC and CO than CDC.

At a load of 5 bar IMEP, CO_2 emissions for PPC were reduced by 9.2% (PPC 30ET) up to 13.9% (PPC 40ET) compared to CDC. PPC with either n-butanol or ethanol not only had less CO_2 emissions than CDC but also had a reduction in carbon available for combustion from nonrenewable fuel sources (ULSD). These reductions were reductions of nonrenewable carbon of 15.3% (PPC 30ET) and 38.8% (PPC 40BU) for a load of 5 bar IMEP.

PPC coupled with the usage of renewably sourced bioalcohols shows a promising method of reducing ICEs environmental impact; however, further optimizations to combustion parameters must be conducted to mitigate UHC and CO emissions.

Acknowledgment

This article is based on work supported by the National Science Foundation Grant No. 1950207.

Contact Information

Dr. Valentin Soloiu, Professor

 $\label{lem:continuous} Director of Automotive and Aerospace Combustion Laboratories \\ Georgia Southern University \\ \underline{vsoloiu@georgiasouthern.edu}$

http://cec.georgiasouthern.edu/engine/

Abbreviations

CI - Compression ignition

CO - Carbon monoxide

CO₂ - Carbon dioxide

COV - Coefficient of variability

CRDI - Common rail direct injection

CVCC - Constant volume compression ignition

D - Bore diameter

DCN - Derived cetane number

DF-PCCI - Dual-fuel premixed charge compression ignition

DI - Direct injection

DTA - Differential thermal analysis

EGR - Exhaust gas recirculation

ESFC - Energy specific fuel consumption

EVC - Exhaust valve closed

EVO - Exhaust valve open

HCCI - Homogeneous charge compression ignition

HTHR - High temperature heat release

IC - Internal combustion

ICE - Internal Combustion Engine

ID - Ignition delay

IMEP - Indicated mean effective pressure

IVC - Intake valve closed

IVO - Intake valve open

LTC - Low temperature combustion

LTHR - Low temperature heat release

LTR - Low temperature release

MFB - Mass fraction burned

N - Engine speed

NOx - Nitrous oxides

PCCI - Premixed charge compression ignition

PFI - Port fuel injection

PM - Particulate matter

PPC - Partially Premixed Combustion

PPRR - Peak pressure rise rate

PRR - Pressure rise rate

RCCI - Reactivity controlled compression ignition

RI - Ringing intensity

RON - Research octane number

S - Stroke

SMD - Sauter mean diameter

SOI - Start of injection

TGA - Thermogravimetric analysis

UHC - Unburnt hydrocarbons

ULSD - Ultra low sulfur diesel

Standard Symbols

AHRR - Apparent heat release rate

ATDC - After top dead center

BTDC - Before top dead center

CD - Combustion duration

CDC - Conventional diesel combustion

References

- Morfeldt, J., Davidsson Kurland, S., and Johansson, D.J.A., "Carbon Footprint Impacts of Banning Cars with Internal Combustion Engines," *Transportation Research Part D: Transport and Environment* 95 (2021): 102807, doi: https://doi.org/10.1016/j.trd.2021.102807.
- Dahodwala, M., Joshi, S., Koehler, E., Franke, M. et al., "Investigation of Diesel-CNG RCCI Combustion at Multiple Engine Operating Conditions," SAE Technical Paper 2020-01-0801, 2020, https://doi.org/10.4271/2020-01-0801.
- 3. D'Ambrosio, S. and Ferrari, A., "Effects of Exhaust Gas Recirculation in Diesel Engines Featuring Late PCCI Type Combustion Strategies," *Energy Conversion and Management* 105 (2015): 1269-1280, doi:10.1016/j.enconman.2015.08.001.
- Sun, C., Martin, J., and Boehman, A.L., "Impacts of Advanced Diesel Combustion Operation and Fuel Formulation on Soot Nanostructure and Reactivity," *Fuel* 276 (2020): 118080, doi:10.1016/j.fuel.2020.118080.
- D'Ambrosio, S., Iemmolo, D., Mancarella, A., and Vitolo, R., "Preliminary Optimization of the PCCI Combustion Mode in a Diesel Engine through a Design of Experiments," *Energy Procedia* 101 (2016): 909-916, doi:10.1016/j. egypro.2016.11.115.

- Rohani, B., Park, S.S., and Bae, C., "Effect of Injection Strategy on Smoothness, Emissions and Soot Characteristics of PCCI-Conventional Diesel Mode Transition," *Applied Thermal Engineering* 93 (2016): 1033-1042, doi:10.1016/j. applthermaleng.2015.09.075.
- Musculus, M.P., Miles, P.C., and Pickett, L.M., "Conceptual Models for Partially Premixed Low-Temperature Diesel Combustion," *Progress in Energy and Combustion Science* 39, no. 2-3 (2013): 246-283, doi:10.1016/j. pecs.2012.09.001.
- 8. Cui, Y., Liu, H., Geng, C., Tang, Q. et al., "Optical Diagnostics on the Effects of Fuel Properties and Coolant Temperatures on Combustion Characteristic and Flame Development Progress from HCCI to CDC via PPC," Fuel 269 (2020): 117441, doi:10.1016/j.fuel.2020.117441.
- Singh, A.P., Kumar, V., and Agarwal, A.K., "Evaluation of Comparative Engine Combustion, Performance and Emission Characteristics of Low Temperature Combustion (PCCI and RCCI) Modes," *Applied Energy* 278 (2020): 115644, doi:10.1016/j.apenergy.2020.115644.
- Pandey, S., Bhurat, S., and Chintala, V., "Combustion and Emissions Behaviour Assessment of a Partially Premixed Charge Compression Ignition (PCCI) Engine with Diesel and Fumigated Ethanol," *Energy Procedia* 160 (2019): 590-596, doi:10.1016/j.egypro.2019.02.210.
- Soloiu, V., Muinos, M., Harp, S., Naes, T. et al., "Combustion and Emissions Characteristics of Dual Fuel Premixed Charge Compression Ignition with Direct Injection of Synthetic FT Kerosene Produced from Natural Gas and Port Fuel Injection of n-Butanol," SAE Technical Paper 2016-01-0787, 2016, https://doi.org/10.4271/2016-01-0787.
- 12. Soloiu, V., Carapia, C.E., Wiley, J.T., Moncada, J. et al., "RCCI Investigations with n-Butanol and ULSD," in ASME 2019 Internal Combustion Engine Division Fall Technical Conference, Chicago, IL, 2019, https://doi.org/10.1115/ ICEF2019-7226.
- Chu, S., Shin, H., Kim, K., Moon, S. et al., "An Experimental Investigation of In-Cylinder Flow Motion Effect on Dual-Fuel Premixed Compression Ignition Characteristics," SAE Technical Paper <u>2020-01-0306</u>, 2020, https://doi.org/10.4271/2020-01-0306.
- Martín, M. and Grossmann, I.E., "Optimal Integration of Renewable Based Processes for Fuels and Power Production: Spain Case Study," *Applied Energy* 213 (2018): 595-610, doi:10.1016/j.apenergy.2017.10.121.
- Morales, M., Quintero, J., Conejeros, R., and Aroca, G., "Life Cycle Assessment of Lignocellulosic Bioethanol: Environmental Impacts and Energy Balance," *Renewable* and Sustainable Energy Reviews 42 (2015): 1349-1361, doi:10.1016/j.rser.2014.10.097.
- Kargbo, H., Harris, J.S., and Phan, A.N., "'Drop-In' Fuel Production from Biomass: Critical Review on Techno-Economic Feasibility and Sustainability," *Renewable and* Sustainable Energy Reviews 135 (2021): 110168, doi:10.1016/j. rser.2020.110168.
- 17. Braz, D.S. and Mariano, A.P., "Jet Fuel Production in Eucalyptus Pulp Mills: Economics and Carbon Footprint of

- Ethanol vs. Butanol Pathway," *Bioresource Technology* 268 (2018): 9-19, doi:10.1016/j.biortech.2018.07.102.
- Shim, E., Park, H., and Bae, C., "Comparisons of Advanced Combustion Technologies (HCCI, PCCI, and Dual-Fuel PCCI) on Engine Performance and Emission Characteristics in a Heavy-Duty Diesel Engine," *Fuel* 262 (2020): 116436, doi:10.1016/J.FUEL.2019.116436.
- Kannan, S., Mahalingam, S., Srinath, S., Sivasankaran, M. et al., "An Experimental Study in HCCI Combustion of LPG in Diesel Engine," *Materials Today: Proceedings* 37, no. Part 2 (2021): 3625-3629, doi:10.1016/J.MATPR.2020.09.774.
- Zehni, A. and Saray, R.K., "Comparison of Late PCCI Combustion, Performance and Emissions of Diesel Engine for B20 and B100 Fuels by KIVA-CHEMKIN Coupling," *Renewable Energy* 122 (2018): 118-130, doi:10.1016/J. RENENE.2018.01.046.
- 21. Okcu, M., Varol, Y., Altun, Ş., and Fırat, M., "Effects of Isopropanol-Butanol-Ethanol (IBE) on Combustion Characteristics of a RCCI Engine Fueled by Biodiesel Fuel," *Sustainable Energy Technologies and Assessments* 47 (2021): 101443, doi:10.1016/J.SETA.2021.101443.
- 22. Taghavifar, H., Nemati, A., Salvador, F.J., and de la Morena, J., "1D Energy, Exergy, and Performance Assessment of Turbocharged Diesel/Hydrogen RCCI Engine at Different Levels of Diesel, Hydrogen, Compressor Pressure Ratio, and Combustion Duration," *International Journal of Hydrogen Energy* 46, no. 42 (2021): 22180-22194, doi:10.1016/J. IJHYDENE.2021.04.035.
- Olmeda, P., García, A., Monsalve-Serrano, J., and Lago Sari, R., "Experimental Investigation on RCCI Heat Transfer in a Light-Duty Diesel Engine with Different Fuels: Comparison versus Conventional Diesel Combustion," *Applied Thermal Engineering* 144 (2018): 424-436, doi:10.1016/J. APPLTHERMALENG.2018.08.082.
- 24. Nishida, K. and Shimizu, H., "Model Based Control for Premixed Charge Compression Ignition Diesel Engine," SAE Technical Paper 2020-01-1150, 2020, https://doi.org/10.4271/2020-01-1150.
- 25. Jia, M., Xie, M., Wang, T., and Peng, Z., "The Effect of Injection Timing and Intake Valve Close Timing on Performance and Emissions of Diesel PCCI Engine with a Full Engine Cycle CFD Simulation," *Applied Energy* 88, no. 9 (2011): 2967-2975, doi:10.1016/j.apenergy.2011.03.024.
- 26. Belgiorno, G., Dimitrakopoulos, N., Blasio, G.D., Beatrice, C. et al., "Parametric Analysis of the Effect of Pilot Quantity, Combustion Phasing and EGR on Efficiencies of a Gasoline PPC Light-Duty Engine," SAE Technical Paper 2017-24-0084, 2017, https://doi. org/10.4271/2017-24-0084.
- Aronsson, H.S., Truedsson, I., Tuner, M., Johansson, B. et al., "Comparison of Fuel Effects on Low Temperature Reactions in PPC and HCCI Combustion," SAE Technical Paper 2014-01-2679, 2014, https://doi.org/10.4271/2014-01-2679.
- 28. Walker M., Hamilton L., Luning-Prak D., and Cowart J., "Increasing High Load Engine Power with Advanced Combustion Modes," SAE Technical Paper Series, 2018, https://doi.org/10.4271/2018-01-0903.

- 29. Dimitrakopoulos, N., Belgiorno, G., Tunér, M., Tunestål, P. et al., "Effect of EGR Routing on Efficiency and Emissions of a PPC Engine," *Applied Thermal Engineering* 152 (2019): 742-750, doi:10.1016/j.applthermaleng.2019.02.108.
- An, Y., Jaasim, M., Raman, V., Pérez, F.E.H. et al., "Homogeneous Charge Compression Ignition (HCCI) and Partially Premixed Combustion (PPC) in Compression Ignition Engine with Low Octane Gasoline," *Energy* 158 (2018): 181-191, doi:10.1016/j.energy.2018.06.057.
- 31. Mao, B., Liu, H., Zheng, Z., and Yao, M., "Influence of Fuel Properties on Multi-Cylinder PPC Operation over a Wide Range of EGR and Operating Conditions," *Fuel* 215 (2018): 352-362, doi:10.1016/j.fuel.2017.08.099.
- 32. Zheng, Z., Chen, P., Yao, M., Liu, X. et al., "Experimental Study on the Partially Premixed Combustion (PPC) Fueled with n-Butanol," *Fuel* 257 (2019): 116000, doi:10.1016/j. fuel.2019.116000.
- 33. Stein, R.A., House, C.J., and Leone, T.G., "Optimal Use of E85 in a Turbocharged Direct Injection Engine," *SAE Int. J. Fuels Lubr.* 2, no. 1 (2009): 670-682, doi:https://doi.org/10.4271/2009-01-1490.
- Liang, M.S., "Assessing Emission and Power Tradeoffs of Biodiesel and n-Butanol in Diesel Blends for Fuel Sustainability," Fuel 283 (2021): 118861, doi:10.1016/j. fuel.2020.118861.
- Gainey, B., Yan, Z., and Lawler, B., "Autoignition Characterization of Methanol, Ethanol, Propanol, and Butanol over a Wide Range of Operating Conditions in LTC/ HCCI," Fuel 287 (2020): 119495, doi:10.1016/j. fuel.2020.119495.
- López, A.F., Cadrazco, M., Agudelo, A.F., Corredor, L.A. et al., "Impact of n-Butanol and Hydrous Ethanol Fumigation on the Performance and Pollutant Emissions of an Automotive Diesel Engine," *Fuel* 153 (2015): 483-491, doi:10.1016/j.fuel.2015.03.022.
- 37. Rakopoulos, C.D., Rakopoulos, D.C., Kosmadakis, G.M., and Papagiannakis, R.G., "Experimental Comparative Assessment of Butanol or Ethanol Diesel-Fuel Extenders Impact on Combustion Features, Cyclic Irregularity, and Regulated Emissions Balance in Heavy-Duty Diesel Engine," *Energy* 174 (2019): 1145-1157, doi:10.1016/j. energy.2019.03.063.
- 38. Lapuerta, M., Hernández, J.J., Fernández-Rodríguez, D., and Cova-Bonillo, A., "Autoignition of Blends of n-Butanol and Ethanol with Diesel or Biodiesel Fuels in a Constant-Volume Combustion Chamber," *Energy* 118 (2017): 613-621, doi:10.1016/j.energy.2016.10.090.
- 39. Rochón, E., Cortizo, G., Cabot, M.I., Cubero, M.T.G. et al., "Bioprocess Intensification for Isopropanol, Butanol and Ethanol (IBE) Production by Fermentation from Sugarcane and Sweet Sorghum Juices through a Gas Stripping-Pervaporation Recovery Process," *Fuel* 281 (2020): 118593, doi:10.1016/j.fuel.2020.118593.
- 40. Calam, A., Aydoğan, B., and Halis, S., "The Comparison of Combustion, Engine Performance and Emission Characteristics of Ethanol, Methanol, Fusel Oil, Butanol, Isopropanol and Naphtha with n-Heptane Blends on HCCI

- Engine," Fuel 266 (2020): 117071, doi:10.1016/j.fuel.2020.117071.
- 41. Nibin, M., Raj, J., and Geo, V., "Experimental Studies to Improve the Performance, Emission and Combustion Characteristics of Wheat Germ Oil Fuelled CI Engine Using Bioethanol Injection in PCCI Mode," *Fuel* 285 (2021): 119196.
- 42. Alternative Fuels Data Center, "Ethanol Feedstocks," accessed June 2, 2022, https://afdc.energy.gov/fuels/ethanol feedstocks.html#:~:text=Today%2C%20nearly%20all%20ethanol%20produced,for%20most%20domestic%20ethanol%20production.
- 43. Aui, A., Wang, Y., and Mba-Wright, M., "Evaluating the Economic Feasibility of Cellulosic Ethanol: A Meta-Analysis of Techno-Economic Analysis Studies," *Renewable and Sustainable Energy Reviews* 145 (2021): 111098, doi:https://doi.org/10.1016/J.RSER.2021.111098.
- 44. Clifford, B.C., "11.3 Economics of Butanol Production—EGEE 439: Alternative Fuels from Biomass Sources," accessed June 2,2022, https://www.e-education.psu.edu/egee439/node/721.
- 45. Elfasakhany, A. and Mahrous, A.-F., "Performance and Emissions Assessment of n-Butanol–Methanol–Gasoline Blends as a Fuel in Spark-Ignition Engines," *Alexandria Engineering Journal* 55, no. 3 (2016): 3015-3024, doi: https://doi.org/10.1016/j.aej.2016.05.016.
- 46. Zheng, Z., Xia, M., Liu, H., Wang, X. et al., "Experimental Study on Combustion and Emissions of Dual Fuel RCCI Mode Fueled with Biodiesel/n-Butanol, Biodiesel/2,5-Dimethylfuran and Biodiesel/Ethanol," *Energy* 148 (2018): 824-838, doi:https://doi.org/10.1016/j.energy.2018.02.015.
- VP Racing, "X98 Public Specification Sheet" VP Racing, 2022, accessed 14 December 2022, doi:https://vpracingfuels.com/wp-content/uploads/2019/12/X98-Spec-Sheets 100419A-1.pdf.
- 48. Hansen, A.C., Zhang, Q., and Lyne, P.W.L., "Ethanol–Diesel Fuel Blends—A Review," *Bioresource Technology* 96, no. 3 (2005): 277-285, doi:https://doi.org/10.1016/j.biortech.2004.04.007.
- 49. Padala, S., Woo, C., Kook, S., and Hawkes, E.R., "Ethanol Utilisation in a Diesel Engine Using Dual-Fuelling Technology," *Fuel* 109 (2013): 597-607, doi: https://doi.org/10.1016/j.fuel.2013.03.049.
- 50. Rakopoulos, D.C., Rakopoulos, C.D., Papagiannakis, R.G., and Kyritsis, D.C., "Combustion Heat Release Analysis of Ethanol or n-Butanol Diesel Fuel Blends in Heavy-Duty DI Diesel Engine," *Fuel* 90, no. 5 (2011): 1855-1867.
- Soloiu, V., Wiley, J.T., Gaubert, R., Mothershed, D. et al., "Fischer-TROPSCH Coal-to-Liquid Fuel Negative Temperature Coefficient Region (NTC) and Low-Temperature Heat Release (LTHR) in a Constant Volume Combustion Chamber (CVCC)," *Energy* 198 (2020): 117288, doi:https://doi.org/10.1016/j.energy.2020.117288.
- 52. Hwang, J., Park, Y., Bae, C., Lee, J. et al., "Fuel Temperature Influence on Spray and Combustion Characteristics in a Constant Volume Combustion Chamber (CVCC) under Simulated Engine Operating Conditions," *Fuel* 160 (2015): 424-433, doi:https://doi.org/10.1016/j.fuel.2015.08.004.

- 53. Tsuji, F.K. and Neto, L.D., "Influence of Vegetable Oil in the Viscosity of Biodiesel A Review," SAE Technical Paper 2008-36-0170, 2008, https://doi.org/10.4271/2008-36-0170.
- 54. Eng, J.A., "Characterization of Pressure Waves in HCCI Combustion," SAE Technical Paper 2002-01-2859, 2002, https://doi.org/10.4271/2002-01-2859.
- Haseli, Y., Entropy Analysis in Thermal Engineering Systems (London, UK: Academic Press, an Imprint of Elsevier, 2020)
- Borman, G. and Nishiwaki, K., "Internal-Combustion Engine Heat Transfer," *Progress in Energy and Combustion Science* 13, no. 1 (1987): 1-46, doi: https://doi.org/10.1016/0360-1285(87)90005-0.
- 57. Soloiu, V., Lewis, J., Yoshihara, Y., and Nishiwaki, K., "Combustion Characteristics of a Charcoal Slurry in a Direct Injection Diesel Engine and the Impact on the Injection System Performance," *Energy* 36, no. 7 (2011): 4353-4371, doi:https://doi.org/10.1016/j.energy.2011.04.006.
- 58. Annand, W.J.D. and Ma, T.H., "Instantaneous Heat Transfer Rates to the Cylinder Head Surface of a Small Compression-Ignition Engine," *Proceedings of the Institution of Mechanical Engineers* 185, no. 1 (1971): 976-987.
- Han, X., Tan, Q., Wang, M., Tjong, J. et al., "Fuel Burn Rate Control to Improve Load Capability of Neat n-Butanol Combustion in a Modern Diesel Engine," SAE Technical Paper 2016-01-2301, 2016, https://doi.org/10.4271/2016-01-2301.
- 60. Soloiu, V., Moncada, J.D., Gaubert, R., Muiños, M. et al., "LTC (Low-Temperature Combustion) Analysis of PCCI (Premixed Charge Compression Ignition) with n-Butanol and Cotton Seed Biodiesel versus Combustion and Emissions Characteristics of Their Binary Mixtures," Renewable Energy 123 (2018): 323-333, doi:10.1016/j. renene.2018.02.061.
- Cheng, X., Li, S., Yang, J., and Liu, B., "Investigation into Partially Premixed Combustion Fueled with n-Butanol-Diesel Blends," *Renewable Energy* 86 (2016): 723-732, doi:https://doi.org/10.1016/j.renene.2015.08.067.

- 62. Zhang, M., Derafshzan, S., Richter, M., and Lundgren, M., "Effects of Different Injection Strategies on Ignition and Combustion Characteristics in an Optical PPC Engine," *Energy* 203 (2020): 117901, doi:https://doi.org/10.1016/j.energy.2020.117901.
- 63. Jain, A., Singh, A.P., and Agarwal, A.K., "Effect of Fuel Injection Parameters on Combustion Stability and Emissions of a Mineral Diesel Fueled Partially Premixed Charge Compression Ignition (PCCI) Engine," *Applied Energy* 190 (2017): 658-669, doi:https://doi.org/10.1016/j.apenergy.2016.12.164.
- Singh, A.P., Jain, A., and Agarwal, A.K., "Fuel-Injection Strategy for PCCI Engine Fueled by Mineral Diesel and Biodiesel Blends," *Energy Fuels* 31, no. 8 (2017): 8594-8607.
- 65. Singh, A.P., Sharma, N., Kumar, V., and Agarwal, A.K., "Experimental Investigations of Mineral Diesel/Methanol-Fueled Reactivity Controlled Compression Ignition Engine Operated at Variable Engine Loads and Premixed Ratios," *International Journal of Engine Research* 22, no. 7 (2020): 2375-2389, doi:https://doi.org/10.1177/1468087420923451.
- 66. Heywood, J., Internal Combustion Engine Fundamentals (New York: McGraw-Hill, 1988)
- 67. Dec, J. and Yang, Y., "Boosted HCCI for High Power without Engine Knock and with Ultra-Low NOx Emissions Using Conventional Gasoline," *SAE Int. J. Engines* 3, no. 1 (2010): 750-767, doi:https://doi.org/10.4271/2010-01-1086.

Appendix A: Additional Materials and Tables

Preliminary Fuel Analysis Methods and Apparatuses

TABLE A.1 Thermophysical properties of research fuels.

	ULSD#2	n-Butanol	X98
LHV [MJ/kg]	45.1	32.0	27.4
DCN*	47.4	16.4	8*
Viscosity at 40°C [cP]	2.52	2.04	1.15
SMD [µm]	21.9	18.74	20.83
Density [g/mL]	0.85	0.81	0.79
TA(10) °C	110	54.3	33.4
TA(50) °C	180	80.8	60.6
TA(90) °C	240	95.4	77.3
Received from literature review			
Chemical formula	C ₁₂ H ₂₃	C ₄ H ₉ OH	C ₂ H ₅ OH
Oxygen [%wt]	_	21.59	34.73
Boiling point [°C]	154-372	117	79
Autoignition temperature [°C]	257	345	366
Latent heat of vaporization [kJ/kg]	585.4	918.42	585.4

Data taken from Refs. [46-51]. © SAE International

Fired Engine Experimental Apparatus and Methods

TABLE A.2 DI timing and injection duration of all combustion experiments conducted.

4 bar IMEP						
Test point	PFI inj. timing [BTDC]	SOI-1 [BTDC]	SOI-1 [ms]	SOI-2 [BTDC]	SOI-2 [ms]	Total time [ms]
CDC	345	NA	NA	13	0.76	0.76
PPC 30BU		60	0.35	7	0.45	0.80
PPC 30ET		60	0.35	9	0.45	0.80
PPC 40BU		60	0.35	5	0.38	0.73
PPC 40ET		60	0.35	10	0.36	0.71
E hay IMED						
5 bar IMEP						
Test point	PFI inj. timing [BTDC]	SOI-1 [BTDC]	SOI-1 [ms]	SOI-2 [BTDC]	SOI-2 [ms]	Total time [ms]
	timing					time
Test point	timing [BTDC]	[BTDC]	[ms]	[BTDC]	[ms]	time [ms]
Test point	timing [BTDC]	[BTDC] NA	[ms] NA	[BTDC] 16	[ms] 0.87	time [ms] 0.87
Test point CDC PPC 30BU	timing [BTDC]	[BTDC] NA 60	[ms] NA 0.35	[BTDC] 16 7	[ms] 0.87 0.53	time [ms] 0.87 0.88

TABLE A.3 DI timing and injection duration of all combustion experiments conducted.

Load [bar]	Combustion test	CoV%
4	CDC	1.692
	PPC 30BU	2.524
	PPC 30ET	3.132
	PPC 40BU	2.614
	PPC 40ET	4.078
5	CDC	1.78
Ilona	PPC 30BU	2.086
erna	PPC 30ET	2.522
VAE International	PPC 40BU	2.600
4	PPC 40ET	2.86

MFB Results

TABLE A.4 MFB at 4 bar IMEP.

	Combustion test	CA10 [CAD]	CA50 [CAD]	CA90 [CAD]	ID [CAD]	CD [CAD]	MAX MFB [%]
_	CDC	4°BTDC	9°ATDC	38°ATDC	9°	44°	96.8
ational	PPC 30BU	2°BTDC	10°ATDC	NA	5°	NA	88.2
erna	PPC 30ET	1°BTDC	11°ATDC	NA	8°	NA	87.3
E Int	PPC 30ET PPC 40BU	2°BTDC	10°ATDC	NA	3°	NA	85.6
© SA	PPC 40ET	1°BTDC	9°ATDC	NA	9°	NA	85.8

TABLE A.5 MFB at 5 bar IMEP.

	Combustion test	CA10 [CAD]	CA50 [CAD]	CA90 [CAD]	ID [CAD]	CD [CAD]	MAX MFB [%]
-	CDC	6°BTDC	9°ATDC	39°ATDC	10°	45°	97.4
tion	PPC 30BU	4°BTDC	9°ATDC	47°ATDC	3°	51°	91.8
terna	PPC 30ET	4°BTDC	9°ATDC	46°ATDC	8°	50°	92.3
in In	PPC 40BU	3°BTDC	9°ATDC	47°ATDC	NA <u>*</u>	50°	92.2
∕S ⊚	PPC 40ET	1°BTDC	9°ATDC	59°ATDC	9°	60°	90.8

^{*} PPC 40BU had an ID of -1° from the autoignition of homogeneous air/fuel mixture (PFI + Pilot Inj.).

Emissions

TABLE A.6 Soot emissions difference at 4 bar and 5 bar IMEP.

Load [bar]	Combustion test	Δ Soot emissions from CDC [g/kWh]	Percent difference from CDC [%]
4	PPC 30BU	-1.362	-84.59
	PPC 30ET	-1.123	-69.75
	PPC 40BU	-1.243	-77.20
	PPC 40ET	-1.519	-94.34
5	PPC 30BU	-0.659	-37.72
	PPC 30ET	-0.745	-42.64
	PPC 40BU	-1.132	-64.79
	PPC 40ET	-1.480	-84.71

TABLE A.7 NOx emissions comparison.

Load [bar]	Combustion test	Δ NOx emissions from CDC [g/ kWh]	Percent difference from CDC [%]	
4	PPC 30BU	-5.68	-38.64	
	PPC 30ET	-4.40	-29.93	
	PPC 40BU	-7.29	-53.33	
	PPC 40ET	-3.00	-20.40	_
5	PPC 30BU	-7.44	-49.60	2
	PPC 30ET	-3.20	-21.33	-
	PPC 40BU	-9.31	-62.06	Caci+cay0+a 1 0
	PPC 40ET	-2.90	-19.33	(

TABLE A.8 Nonrenewable fuel carbon available at 4 bar and 5 bar IMEP.

Load [bar]	Combustion test	Carbon available from DI ULSD [%]	Carbon available from renewable PFI fuel [%]	# of moles of carbon available from fuel [mol/h]	∆% of carbon from ULSD from CDC [%]
4	CDC	100	0%	65.8	_
	PPC 30BU	76	24	71.2	-17.8
	PPC 30ET	79	21	68.9	-17.3
	PPC 40BU	65	35	71.0	-29.9
	PPC 40ET	67	32	69.0	-29.7
5	CDC	100	0	84.5	_
	PPC 30BU	75	25	86.1	-23.6
	PPC 30ET	83	17	86.2	-15.3
	PPC 40BU	63	37	82.1	-38.8
	PPC 40ET	68	32	83.0	-33.2

SAE IIIEIII

[©] 2023 SAE International. All rights reserved. No part of this publication may be reproduced, stored in a retrieval system, or transmitted, in any form or by any means, electronic, mechanical, photocopying, recording, or otherwise, without the prior written permission of SAE International.